

X-62 84539

522

Copy
RM E57120

NACA RM E57120

CLASSIFIED-AUTHORITY-MEMO.US:
13. TAINÉ TO SHAUKLAS
DATED JUNE 15, 1967

Declassified by authority of NASA
Classification Change Notices No. 113
Dated ** 6/2-8/67

NACA

RESEARCH MEMORANDUM

EXPERIMENTAL BEHAVIOR OF PENTABORANE-AIR COMBUSTION
PRODUCTS DURING EXPANSION IN A CONVERGENT -
DIVERGENT NOZZLE

By J. Robert Branstetter and Paul C. Setze

Lewis Flight Propulsion Laboratory
Cleveland, Ohio

GPO PRICE \$ _____

CFSTI PRICE(S) \$ _____

Hard copy (HC) 3.00

Microfiche (MF) .65

ff 653 July 65

FACILITY FORM 602

N67-31730

(ACCESSION NUMBER)

69

(PAGES)

(THRU)

(CODE)

33

(CATEGORY)

(NASA CR OR TMX OR AD NUMBER)

for the National Defense of the United States within the meaning

NATIONAL ADVISORY COMMITTEE
FOR AERONAUTICS

WASHINGTON

February 18, 1958

NACA RM E57I20

SECRET

TABLE OF CONTENTS

	Page
SUMMARY	1
INTRODUCTION	1
APPARATUS AND EXPERIMENTAL PROCEDURE	3
Apparatus	3
General assembly	3
Combustor and nozzle	3
Fuel injectors	4
Fuel systems	4
Fuels	4
Instrumentation	4
Experimental Procedure	5
ANALYTIC PROCEDURE	6
Derivation of Equations	6
Applications of Equations	12
Use of calibration data	12
Pentaborane performance analysis	13
PRESENTATION OF RESULTS	15
ANALYSIS OF RESULTS	17
Symmetry of Flow in Nozzle	17
Behavior of Liquid Boric Oxide in Nozzle	17
Abrupt Condensation Phenomena	18
Effect of Abrupt Condensation on Performance	21
Comparison of Experimental Results with Several Ideal Models	22
Effect of Oxide Films	24
SUMMARY OF RESULTS	27
APPENDIXES	
A - SYMBOLS	29
B - ACCURACY OF EXPERIMENTAL RESULTS	32
C - COMBUSTION EFFICIENCY	34
D - ERRORS IN THRUST COMPUTATIONS DUE TO NON-IDEAL EXPANSION IN NOZZLE CONVERGENCE	37
REFERENCES	39

4533

SECRET

RESEARCH MEMORANDUM

NATIONAL ADVISORY COMMITTEE FOR AERONAUTICS

RESEARCH MEMORANDUMEXPERIMENTAL BEHAVIOR OF PENTABORANE-AIR COMBUSTION PRODUCTS
DURING EXPANSION IN A CONVERGENT-DIVERGENT NOZZLE

By J. Robert Branstetter and Paul C. Setze

SUMMARY

In order to evaluate the postcombustion behavior of boric oxide, pentaborane-air mixtures, burned to completion at a combustor pressure of 3 atmospheres, were expanded through a 7.1-inch-long convergent-divergent nozzle having a 4-inch-diameter throat and an exit-to-throat area ratio of 1.68. The experimentally determined thrust performance was in good agreement with the ideal equilibrium performance at stagnation temperatures of 3300° R and lower. The boric oxide vapor at the combustor exit required about 400 Fahrenheit degrees supercooling before any condensed phase was observed. For a given thrust, fuel consumption was as much as 20 percent greater than predicted from vapor-pressure data for combustor-outlet temperatures in the vicinity of 3600° R. A similar result could be expected in full-scale engines, since the test combustor provided an unusually long dwell time and a highly turbulent environment. During the expansion process, the vapor (when present) did not condense to the extent predicted for an equilibrium expansion process. Moreover, condensation was observed only in the form of small, abrupt phase changes in the subsonic flow near the throat. Friction, due to liquid boric oxide films on the nozzle surfaces, was negligible when the surface temperature was above 800° F.

INTRODUCTION

Special fuels that show promise of extending range, thrust, and operational limits of jet-propelled aircraft are being investigated at the NACA Lewis laboratory. Boron hydride fuels appear attractive because of high heats of combustion and desirable chemical reactivity; for example, pentaborane has a heating value of 29,100 Btu per pound. At first glance, however, the heating value of this and other boron-containing compounds can be misleading. Thus, at normal turbojet primary-combustor operating temperatures, the primary combustion product, boric oxide (B_2O_3), is in the liquid phase; but, in a ramjet or afterburning turbojet operating at

high temperatures, the boric oxide is in the vapor phase and has absorbed a large amount of energy in the process of vaporization. A comparison (ref. 1) of the specific fuel consumption of pentaborane and octene-1 for an ideal combustor with a choked convergent nozzle shows how vaporization increases the specific fuel consumption $sfc ((lb \text{ fuel})/(hr)(lb \text{ thrust}))$:

Combustion temperature, °R	Vaporized B_2O_3	Pentaborane sfc
	Total B_2O_3	Hydrocarbon sfc
2800	0	0.72
3800	1	.84

These calculations were based on the assumptions of one-dimensional frictionless flow, boric oxide phase equilibrium at the combustor exit, and no phase change through the nozzle. The liquid boric oxide, when present, was assumed to be in thermal and velocity equilibrium with the rest of the combustion products.

Analyses such as the one just described are the yardsticks by which the merits of jet-engine fuels are measured. Minor changes in the assumptions or in a thermodynamic property used in the calculations can yield major changes in the thrust and specific-fuel-consumption results for boron-containing fuels.

To assist in the analyses of the performance of boron-containing fuels, a series of carefully controlled experiments was initiated. The behavior of the combustion products on leaving the combustor and passing through a convergent-divergent nozzle was measured. Knowledge gained from these tests will provide information on the processes of flow and expansion that take place when boron-containing fuels are burned in a full-scale engine.

The primary objectives of the work described in this report are to determine:

- (1) Whether liquid boric oxide particles remain in thermal and velocity equilibrium with the rest of the combustion products during expansion through a convergent-divergent nozzle.
- (2) The magnitude of any deviation from phase equilibrium exhibited by the boric oxide at the combustor exit. (Phase equilibrium is based on the most generally accepted vapor-pressure data of boric oxide (ref. 2).)
- (3) The nature and extent of boric oxide phase changes in a convergent-divergent nozzle.

SECRET

(4) The loss in nozzle performance due to oxide films adhering to nozzle surfaces.

A difficult part of this work was the development of apparatus and techniques accurate enough to conduct an investigation of the type described. Also, techniques for conserving scarce pentaborane had to be devised.


Pentaborane-air mixtures were burned to near completion, and the combustion products were discharged through a 7.1-inch-long convergent-divergent nozzle having a 4-inch-diameter throat. The exit Mach number was approximately 2. The nozzle was instrumented and carefully calibrated with heated air. The tests were conducted at a combustor pressure of approximately 3 atmospheres and were confined to equivalence ratios below the region of appreciable dissociation. The range of equivalence ratios was chosen so that data could be obtained for boric oxide completely, partially, or negligibly vaporized at the combustor exit. Experimentally determined performance values were obtained for these conditions and were compared with the results of several conventional theoretical analyses.

APPARATUS AND EXPERIMENTAL PROCEDURE

Apparatus

General assembly. - A diagram of the experimental equipment is shown in figure 1. Combustion air, at approximately 5 atmospheres pressure and ambient temperature, was critically throttled by a remotely operated valve and passed through a single can-type jet-engine combustor used as a preheater. An insulated duct downstream of the preheater contained baffles that evened the velocity profile and produced small-scale turbulence at the entry to the fuel injector. The combustion products discharged through the exhaust nozzle into a thrust barrel supported by flexible straps fastened to the top of the exhaust plenum. The exhaust gases, after being cooled to near ambient temperature, discharged into an exhaust duct that was maintained at about $1/3$ -atmosphere pressure.

Combustor and nozzle. - The combustor and the nozzle were fabricated separately and welded to a common flange that was bolted to the exit plenum (fig. 2). The combustor was $8\frac{3}{8}$ inches in diameter and 36 inches long. Cooling air was metered and fed into an annular passage surrounding the combustor by four ducts spaced 90° apart. The nozzle was machined from a billet of mild steel and its internal surfaces were nickel-plated to avoid corrosion. The nozzle was cooled by operating it as a heat sink; this cooling principle was satisfactory only because the tests were of short duration. During the investigation, the downstream portion of the nozzle block was cored (as shown in fig. 2) to obtain a more uniform surface temperature.



Fuel injectors. - Two fuel injectors were used. Fuel injector A, used in the first portion of the program, is shown in figure 3. The pentaborane fuel-injector bars were coplanar with the upstream edge of a row of V-gutters. The spacing between the gutters and between the injector bars was 1.25 inches. Simple orifices, spaced every 1.25 inches along each bar, injected the fuel downstream between the V-gutters. The V-gutters blocked 72 percent of the area of the duct and thereby appreciably accelerated the pentaborane-air mixing process. Warmup fuel (propylene oxide or JP-4) could be injected into the shelter of the V-gutters by the stub-tube orifices protruding into the combustor.

Several remarks concerning fuel-injector design and performance will help to explain the selection of fuel injector B, shown in figures 4 and 5, as the injector used in the majority of the tests. Fuel injector A provided satisfactory combustion efficiencies only at the leaner equivalence ratios investigated. Fuel injector B was designed to obtain strong and uniform mixing of the pentaborane-air mixture prior to combustion, on the premise that this is a prerequisite for high combustion efficiencies. This fuel injector gave the desired results and therefore was used throughout the latter portion of the program. Details of the injector are shown in figure 4. Atomizing air at near sonic velocity atomized the fuel to a fine mist, which was directed downstream at a 40° angle toward the combustor axis. The mainstream air was accelerated by blocking off about 88 percent of the duct area with plates inserted between the spray bars (fig. 5). The fuel injector was water-cooled, so that pentaborane fuel flow could be initiated while the preheater was operating.

Fuel systems. - The fuel systems and the method for supplying air for atomization of the fuel are shown in figure 6. The test-fuel system was flushed with dry JP-4 fuel immediately after each pentaborane test was concluded.

Fuels. - The test fuel, pentaborane (B_5H_9), had the following properties:

Heat of combustion (H_2O vapor, B_2O_3 crystal), Btu/lb	29,100
Stoichiometric fuel-air ratio	0.0763
Pounds of boric oxide per pound of fuel	2.76

Propylene oxide and JP-4 fuel (warmup fuels) were used interchangeably for calibrating the apparatus and for warmup prior to the pentaborane tests.

Instrumentation. - The combustion air, atomizing air, and cooling air were metered by sharp-edged orifices conforming to ASME standards. Pentaborane fuel-flow rates were sensed by two rotating-vane flowmeters, each of which was connected to a separate continuous recorder. Dual

instrumentation was omitted for the warmup fuel. Barrel thrust was measured by a strain gage connected to a continuous recorder. A camera recorded at 5-second intervals the manometer-board readings, which consisted of orifice differential pressures, static pressures (stations shown in fig. 2), combustor-inlet total pressure, and exhaust-plenum pressure.

Thermocouple data from the air orifices, fuel meters, combustor inlet (station 2), combustor walls (fig. 2), and cooling-air discharge were recorded every 6 seconds on self-balancing potentiometers. Temperature data from two longitudinal rows of nozzle-wall thermocouples were recorded at 6-second intervals, while data from the other two rows were obtained from an indicating potentiometer. At the lower equivalence ratios investigated, radial-temperature profiles of the combustion products were obtained by means of a traversing thermocouple connected to a fast-response, self-balancing recording potentiometer. The thermocouple, which was mounted 8 inches upstream of the nozzle entry, required 30 seconds to travel from the wall to the center of the combustor and back again to the wall. A calibrated, sonic-flow aspirating thermocouple (ref. 3) was used for the calibration tests. This thermocouple was replaced with an exposed-bead thermocouple for the pentaborane tests.

Samples of the pentaborane combustion products were obtained with a liquid-nitrogen-cooled probe immersed in the stream. Solids were trapped on a glass wool gauze, and the filtered gases flowed into an evacuated bottle. Operation of the apparatus was controlled by a remotely operated valve.

Experimental Procedure

Each test was conducted in the following manner: The pentaborane flowmeters and the thrust-barrel strain gage were calibrated. The combustion airflow was established, and warmup fuel was introduced at the preheater (and also through the warmup-fuel orifices of fuel injector A when this injector was used). Complete sets of data were taken at various fuel-air ratios that yielded combustor-outlet temperatures ranging from 600° to 2500° F. Flow rates were adjusted to maintain a combustor pressure of approximately 3 atmospheres. The data obtained in this manner were used to calibrate the apparatus. During the calibration, all instruments were checked for proper functioning, and the apparatus was tested for leaks. Next, the apparatus was cooled, and the sonic-flow aspirating thermocouple was replaced with the open-bead thermocouple.

In order to minimize the consumption of pentaborane, the combustor was preheated prior to injection of the test fuel. When the uncooled fuel injector A was used, preheat was obtained solely from the injection of warmup fuel into the shelter of the V-gutters. Preheat for fuel

injector B was provided by the preheater. In either case, as soon as the pentaborane fuel flow was established, the warmup fuel was shut off. Air- and fuel-flow rates were quickly adjusted to predetermined values, and data were taken at these fixed flow rates for a period of at least 30 seconds. On most runs, the fuel-air ratio was then changed to a new value, and the test was continued until the fuel was expended. In many cases, a combustion-product sample was obtained during the run. Sampling of the products, which required about 20 seconds, was begun shortly after the fuel-air ratio was set. (The samples were quantitatively analyzed for free hydrogen and free boron.)

After each test, the combustor, the nozzle, and the fuel injector were inspected and thoroughly cleaned. Measurements of the nozzle-throat diameter determined the amount of residual shrinkage sustained by the nozzle.

ANALYTIC PROCEDURE

Derivation of Equations

The three principal quantities calculated from the data were combustion efficiency η_c , thrust at the nozzle throat F_8 , and thrust at the nozzle exit F_{15} . The symbols used in deriving these quantities are listed in appendix A.

The combustion efficiency is obtained from continuity considerations. In general, the total weight rate of mass transfer is

$$w_t = \frac{\rho AV}{144} \quad (1)$$

For ideal one-dimensional flow at the nozzle throat, substitution of

$$\rho = \frac{144p}{Rt} \quad (2)$$

and

$$V_8 = a = \sqrt{\gamma g R t}_8 \quad (3)$$

into equation (1) yields

$$w_t = \left(p A \sqrt{\frac{\gamma g}{R t}} \right)_8 \quad (4)$$



By using the relations for the ratio of total to static temperature

$$T/t = 1 + \frac{\gamma - 1}{2} M^2 \quad (5a)$$

and the ratio of total to static pressure

$$P/p = \left(1 + \frac{\gamma - 1}{2} M^2 \right)^{\frac{\gamma}{\gamma - 1}} \quad (5b)$$

equation (4) becomes

$$w_t = \left(\frac{P A Y^*}{\sqrt{R T}} \right)_8 \quad (6)$$

where

$$Y^* = \sqrt{\frac{\gamma g}{\left(\frac{\gamma + 1}{2} \right)^{\frac{\gamma + 1}{\gamma - 1}}}}$$

The gamma factor Y^* is plotted in figure 7(a). For real flow, the nominal area A_n requires correction factors that account for boundary-layer film and nozzle-wall curvature C_d , and thermal contraction of the wall C_k . The coefficient C_d was computed by means of reference 4 and is presented in figure 8. The coefficient C_k was obtained by actual calibration of the nozzle. Setting

$$A = A_n C_k C_d$$

and making use of the fact that, in an isentropic expansion, the total pressure is the same throughout the nozzle, equation (6) is solved for the total temperature at the throat:

$$T_8 = \frac{(P_4)^2}{R_8} \left(\frac{A_n C_d C_k Y^*}{w_t} \right)_8^2 \quad (7)$$

The properties R and γ change with the amount of liquid and vapor present in the mixture as well as with the equivalence ratio:

$$R = R_g \frac{w_g}{w_t} = R_g \left(1 - \frac{w_l}{w_t} \right) \quad (8)$$

and

$$r = \frac{\sum n C_p}{\sum n C_p - 1.987 \sum n g} \quad (9)$$

where the sum is taken over components of the mixture. Equations (8) and (9) are developed basically in the same manner as given in reference 5. The quantities involved are evaluated at the static temperature of the throat (eq. (5)):

$$t_8 = \left(\frac{2T}{r + 1} \right)_8 \quad (5c)$$

The combustion efficiency is defined as the enthalpy rise across the combustor divided by the heat of combustion:

$$\eta_c = \frac{H_8 + \left(h_v \frac{w_l}{w_a} \right)_8 + \frac{Q}{w_a} - H_3}{h_c (f/a)} \quad (10)$$

The basis taken is 1 pound of air. The term Q accounts for the heat transferred to the coolant between stations 3 and 8, and the term H_8 does not include the latent heat of vaporization of the oxide.

Equations (4) to (10) permit the evaluation of T_8 and η_c when the fraction of boric oxide in the vapor state is known. Conversely, equation (10) can be used to determine the ratio of liquid to vapor oxide if η_c is 100 percent.

The thrust at any point in the nozzle can be expressed as a sum of a pressure term and a momentum term:

$$F = pA + \frac{w_t V}{g} \quad (11)$$

Applying equations (1) to (3), this reduces to

$$F = pA(1 + rM^2) \quad (11a)$$

The ideal one-dimensional stream thrust at the nozzle throat is obtained by changing to total pressure by means of equation (5b) and by noting that, at the throat (station 8), M equals 1. Then,

$$F_{8,id} = (PAZ^*)_8 \quad (12)$$

where

$$Z^* = \frac{\gamma}{2\gamma-1}(\gamma + 1)^{\frac{1}{1-\gamma}}$$

The gamma factor Z^* is plotted in figure 7(b). To correct for real flow, the nominal area A_n is multiplied by coefficients C_k (for thermal contraction of the nozzle wall) and C_m (for boundary-layer effects and nozzle-wall curvature).

$$F_8 = P_4(A_n C_m C_k Z^*)_8 \quad (13)$$

where, again, use is made of the isentropic expansion property, P_4 equals P_8 . The coefficient C_m is computed by means of reference 4 and is presented in figure 8.

The ideal one-dimensional stream thrust at the exit (station 15), by means of equation (11a), becomes

$$F_{15,id} = [pA(1 + \gamma M^2)]_{15} \quad (14)$$

This may be expressed in terms of

$$\Delta F_{id} = F_{15,id} - F_{8,id}$$

$$F_{15,id} = F_{8,id} \left[1 + \left(\frac{\Delta F}{F_8} \right)_{id} \right] \quad (14a)$$

The ratio of the ideal one-dimensional thrust change between the nozzle throat and exit to the ideal thrust at the throat, $(\Delta F/F_8)_{id}$, is a function of the expansion ratio of the nozzle A_{15}/A_8 and the ratio of the specific heats of the products only. Figure 9 presents $(\Delta F/F_8)_{id}$ as a function of γ for A_{15}/A_8 equal to 1.68.

Equation (14a) for real flow becomes

$$F_{15} = F_8 \left(1 + \frac{\Delta F}{F_8} \right) \quad (15)$$

Values of $\Delta F/F_8$ are considerably smaller than $(\Delta F/F_8)_{id}$ because of wall friction and three-dimensional flow losses. The friction loss for

gaseous flow was computed from the equations of reference 6 by using experimentally determined values of gas and nozzle-wall temperature. Friction in the nozzle divergence is proportional to the ideal thrust change:

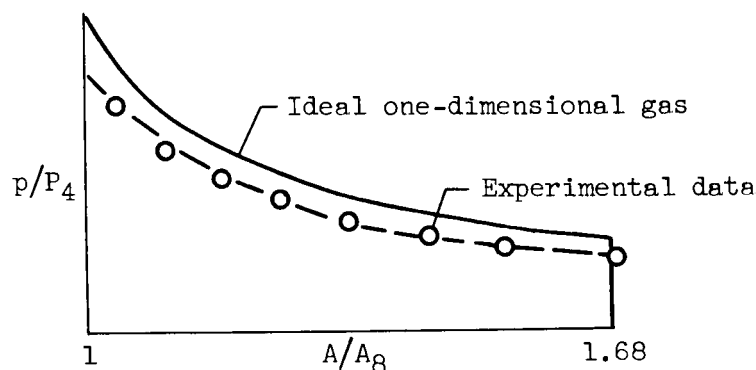
$$\text{Friction} = C_{fr} (\Delta F_{id}) \quad (16)$$

Figure 8 presents the friction coefficient C_{fr} as a function of the primary variable, gas temperature.

The thrust loss that occurs in the divergence as a result of non-uniform expansion of the gases can be determined as follows: For one-dimensional ideal flow,

$$\Delta F_{id} = \left(\int_{A_8}^{A_{15}} p \, dA \right)_{id} = P_4 A_8 \int_{A/A_8 = 1}^{A/A_8 = 1.68} \left(\frac{p}{P_4} \right)_{id} d \left(\frac{A}{A_8} \right) \quad (17)$$

The quantity under the integral $\int_{A/A_8 = 1}^{A/A_8 = 1.68}$ is equivalent to the area under the ideal curve as shown in the following diagram:



Likewise, the area under the experimentally determined curve represents the actual pressure force acting on the divergent surface of the nozzle. Therefore, at a given value of P_4 ,

$$\frac{\text{Area under experimental curve}}{\text{Area under ideal curve}} = \frac{\int_{A_8}^{A_{15}} p \, dA}{\left(\int_{A_8}^{A_{15}} p \, dA \right)_{id}} \quad (18)$$

is the ratio of the actual to ideal pressure forces. The notation used in equation (18) can be simplified by letting

$$\int_{A_8}^{A_{15}} p \, dA = \Sigma pA \quad (19a)$$

and

$$\left(\int_{A_8}^{A_{15}} p \, dA \right)_{id} = \Delta F_{id} \quad (19b)$$

Note that the actual thrust change is less than ΣpA by an amount equal to the friction force:

$$\Delta F = \Sigma pA - \Delta F_{id} C_{fr} \quad (19c)$$

Divergence efficiency is defined as

$$\eta_w = \left(\frac{\Sigma pA}{\Delta F_{id}} \right) 100 \quad (20)$$

The term ΔF_{id} is a function of γ , which for the actual gas increases when the gas expands. The calculation of ΔF_{id} can be simplified without an objectionable error by evaluating ΔF_{id} for a frozen value of γ equal to γ_8 computed for the experimental data.

A useful equation for the actual stream thrust can now be obtained. From equations (15) and (19c),

$$F_{15} = F_8 + \Sigma pA - \Delta F_{id} C_{fr} \quad (21)$$

Substituting equations (13) and (20) in equation (21) yields

$$F_{15} = (A_n C_m C_k Z^*)_8 P_4 + \Delta F_{id} (\eta_w / 100 - C_{fr}) \quad (22)$$

Introducing equation (12) in the form of $F_{8,id} = P_4 (A_n C_k Z^*)_8$,

$$F_{15} = P_4 (A_n C_k Z^*)_8 [C_m + (\Delta F / F_8)_{id} (\eta_w / 100 - C_{fr})] \quad (23)$$

which gives actual stream thrust in terms of real gas properties.

An alternative means of determining the thrust at the nozzle exit is the use of the thrust barrel. The thrust as determined by the thrust barrel, $F_{15,bb}$, is the sum of the strain-gage force and a much smaller force stemming from the axial body forces acting on the outer surface of the thrust barrel. The subscript bb will be used throughout the report to differentiate between the two methods of evaluating the nozzle-exit stream thrust.

Applications of Equations

Use of calibration data. - The flow calibration data were used to determine

- (1) Shrinkage of the nozzle-throat area C_k
- (2) Divergence efficiency of perfect gases in the nozzle divergence η_w
- (3) Accuracy of T_8 , η_c , F_8 , F_{15} , and $F_{15,bb}$ for completely gaseous exhaust products.

The following information was obtained for each calibration run: (1) airflow rate, (2) warmup-fuel rate, (3) thrust-barrel force, (4) rate of heat rejection to the coolant, (5) nozzle-throat area at 70° F, A_n , and (6) a complete set of temperature and pressure data. The aspirating thermocouple data showed that the temperature profile at the combustor exit was very flat. The stagnation temperature of the gases at the nozzle throat (T_8) was computed on the basis that half the heat rejected from the combustor occurred between the traversing-thermocouple station and the throat. Therefore,

$$T_8 = T_{\text{probe}} - \frac{1}{2} \frac{Q}{w_a c_{p,8}} \quad (24)$$

The last term of the equation is less than 1 percent, because the cooling air was carefully regulated to ensure only enough heat transfer to prevent damage to the apparatus.

The coefficient C_k was determined by inserting the data of the calibration flow tests into equation (7). Values of C_k for a range of nozzle-wall temperatures are shown in figure 10.

Nozzle-divergence efficiency values η_w were obtained as follows: For each test, p/P_4 values were plotted in the manner shown in figure 11.



The area under the curve from the nozzle throat to the nozzle exit was planimetered, and η_{ω} was computed in the manner described in equations (18) to (20). The results, shown in figure 12, are somewhat dependent on γ . Therefore, the data curve has been extrapolated into a region of low values of γ in order to permit comparison of the calibration and pentaborane data.

Nozzle-pressure-ratio data, plotted as a function of γ_8 , aided in defining the flow characteristics of the nozzle. Several of these plots are shown in figure 13. From these and similar plots, curves of p/P_4 against A/A_8 can be generated for any desired value of γ_8 .

Over-all accuracy of the principal performance quantities, when applied to the flow of gases, was obtained from an analysis of the calibration data. The results of this analysis are included in the discussion of experimental accuracy presented in appendix B.

Pentaborane performance analysis. - If equation (10) and all other equations containing terms affected by the composition of the combustion products are to be solved, the ratio of vaporized to total boric oxide must be known. Although a 100-percent error in the aforementioned ratio will yield an insignificant error in the value of F_8 and F_{15} , the assignment of a portion of the oxide to the wrong phase yields an appreciable error in the combustion-efficiency data. For example, the computed η_c values will be 1 percent low for each 7 percent of the oxide that is assumed to be liquid when it is actually a vapor.

Two basic methods are available for determining the amount of vaporized boric oxide. In the conventional method, the amount of oxide vapor is defined by the ideal equilibrium vapor-pressure data. Because this method makes the oxide phase and the combustion efficiency dependent on the vapor-pressure data (ref. 2), an indirect method of making the determination was used. The boric oxide was assumed to be all in the liquid phase at the lowest equivalence ratios tested and all in the vapor phase at the highest equivalence ratio tested. These assumptions permitted a direct solution of all the equations. The computed combustion efficiencies for pentaborane at both the lowest and highest equivalence ratios tested fell between 99 and 103 percent. Complete combustion was therefore assumed throughout and included the intermediate values of equivalence ratio where the boric oxide was in a mixed phase at the nozzle throat. Since the combustion efficiency was fixed at 100 percent, the amount of oxide in each phase could be computed by a trial-and-error solution of equations (7) to (10).

Thrusts at the nozzle exit, as measured by the two separate methods of pressures and thrust barrel, were subject to certain limitations. Equation (23) for F_{15} is applicable, provided the oxide film on the nozzle surfaces does not alter the area of the throat or the value of C_{fr} , since both items were computed for gas flow only. Thrust values obtained from the thrust barrel are applicable for even the thickest films. Therefore, a comparison of F_{15} (values from eq. (23)) and $F_{15,bb}$ provides a means of measuring the effect of the films on thrust. Also, the two methods provide a check on the accuracy of the data as a whole. Appendix B notes that the $F_{15,bb}$ data were less precise than the F_{15} data; consequently, the F_{15} values are of the greater accuracy when oxide films are not an influencing factor. However, care must be exercised in interpreting the F_{15} data, since equation (23) assumes that (1) the liquid particles remain in temperature and velocity equilibrium with the gas stream during subsonic expansion, and (2) no condensation occurs in the subsonic portion of the nozzle.

In order to clarify the comparison between the experimental data and the theoretical data, the experimental data were reduced to a base of unit airflow, constant inlet-air temperature, and no friction on the divergent portion of the nozzle. The theoretical data were corrected for three-dimensional flow in the nozzle. The methods used are as follows:

(1) Thrust based on unit airflow is

$$S_a = F_8 / w_a \quad (25)$$

$$S_{a,id} = \frac{F_{8,id}}{w_a} = \frac{[pA(1 + r)]_{8,id}}{w_a} = \left(1 + \frac{f}{a}\right) \left[\sqrt{\frac{Rt}{rg}} (r + 1)^2 \right]_8 \quad (26)$$

(2) Data were reduced to an inlet-air temperature of 360° R by using the following equations:

$$t_{8,corr} = t_8 + \left[\left(360 - T_3 + \frac{Q}{w_t c_{p,3}} \right) \frac{c_{p,3}}{c_{p,8}} \right] \frac{2}{r_8 + 1} \quad (27)$$

and, from equation (26),

$$S_{a,corr} = S_a \sqrt{\frac{t_{8,corr}}{t_8}} \quad (28)$$

The terms in parentheses in equation (27) treat the heat that is rejected to the cooling air as equivalent to a drop in inlet-air temperature.

(3) The deletion of friction was treated by simply dropping the C_{fr} term in equation (23). This was done because C_{fr} applies only to the friction produced by clean walls; whereas the actual friction, which is dependent on the boric oxide film, may be appreciably greater. The nozzle-exit specific thrust then becomes, by multiplying equation (23) by the correction factor of equation (28) and dividing by w_a ,

$$\frac{F_{15,corr}}{w_a} = \frac{(A_n C_k Z^*)_8}{w_a} P_4 \sqrt{\frac{t_{8,corr}}{t_8}} \left[C_m + \left(\frac{\Delta F}{F_8} \right)_{id} \frac{\eta_w}{100} \right] \quad (29)$$

(4) The ideal one-dimensional equation (14a) was corrected to three-dimensional flow by assigning a value of 79 to η_w ; this value was determined from the calibration tests. From equations (14a), (20), and (26), with η_w equal to 79, the ideal three-dimensional specific thrust becomes

$$\left(\frac{F_{15}}{w_a} \right)_{id} = S_{a,id} \left[1 + 0.79 \left(\frac{\Delta F}{F_8} \right)_{id} \right] \quad (30)$$

PRESENTATION OF RESULTS

The data and results presented in this section, unless specifically indicated, were subject to a thorough screening in order to ensure that (1) combustion of the pentaborane was nearly complete, and (2) the presence of oxide films on the nozzle surfaces did not give misleading results.

Item (1) was dictated by the principal goal of this program; namely, the evaluation of the postcombustion behavior of boric oxide in the test apparatus. A prerequisite was the development of a fuel injector that permitted complete, or nearly complete, combustion of the pentaborane. The technique for achieving good combustion at the fuel-air ratios and operating conditions investigated herein was discussed in the section on apparatus. The fact that nearly 100-percent combustion efficiency was obtained is substantiated, in part, by the analysis of the combustion-product samples extracted by means of the sampling probe. Only traces of free boron were found for the tests presented in the tables. (Samples were not obtained during several of the tests at the intermediate fuel-air ratios, because the sampling probe failed because of excessive temperatures.) In contrast to the low free-boron content observed for the data presented, large quantities of free boron were measured when a fuel injector producing low combustion efficiency was tested. Appendix C presents

additional evidence that combustion was nearly complete for the data presented. Since much of this evidence is based on the ANALYSIS OF RESULTS section, the discussion of results should be read before turning to the appendix.

Item (2) was important because oxide films of appreciable thickness affected the measurement of the mainstream flow behavior. Thick films, by reducing the effective nozzle-throat area, affected the computed thrust and combustion-efficiency values. Also, the accuracy of the pressure data was somewhat impaired when films were very viscous. Whenever oxide films were judged to be yielding a data error in excess of the error limits (appendix B), the data were not presented in the tables. Some of the tests discarded because of the presence of thick films yielded data of sufficient reliability to permit a study of the effect of oxide films on performance. These results, along with the computation method used, are presented in the ANALYSIS OF RESULTS.

Primary data for the six tests subjected to a comprehensive analysis are given in tables I and II. These data were obtained during the last 10 seconds of the test for each fuel-air ratio investigated. During this 10-second period, the fuel flow, airflow, and system pressures were within 1 percent of being constant. Stream-thrust values, obtained by means of the thrust barrel, were usually within 2 percent of being constant. Combustor-wall temperatures and the cooling-air discharge temperature were close to equilibrium values; nozzle-wall temperatures were beginning to level off.

Combustor-exit temperature profiles, obtained at the two leanest fuel-air ratios investigated, are presented in figure 14. Although these data do not contain a correction for heat-transfer loss, the data error is judged to be smaller than would be the case for liquid-free combustion products.

Pentaborane performance results for the six data points of tables I and II are presented in table III. These results, computed by the method described in the ANALYTIC PROCEDURE section, are used in figures 15 to 18 as follows:

Figure 15 presents nozzle-pressure-ratio data for the pentaborane tests and the calibration tests described in the ANALYTIC PROCEDURE. (Although an abscissa scale for nozzle-area ratio is customary for this type of plot, a nozzle-length scale was used in order to keep the curves from bunching at the throat as in fig. 11.) The pentaborane data in figure 15 indicate that flow separation existed downstream of station 13. This separation resulted from an overloaded and, hence, a too highly pressurized exhaust system. Separation did not appear to be related to the fuel being tested, and the effects of separation on total stream thrusts are negligible; however, the axial force exerted on the divergence

itself was increased several percent by the flow separation. For the purposes of this report, performance results are of more fundamental value when the nozzle divergence force is evaluated on the basis of unrestricted expansion of the products. For this reason, the presence of separated flow is ignored in both the faired data curves of figure 15 and the calculated data.

Figure 16 presents nozzle-throat data for static temperature, specific impulse, and percent boric oxide condensed; figure 17 presents nozzle-exit data for air specific thrust. The ideal data, shown for comparison purposes, are for the two limiting cases where the boric oxide is in a single phase while passing through the nozzle. These data were computed by the method described in the calculation procedure (see eqs. (26) and (30)).

Figure 18 presents nozzle divergence efficiency and efficiency ratio for both the pentaborane tests and the calibration tests.

ANALYSIS OF RESULTS

Symmetry of Flow in Nozzle

Before the results are analyzed in detail, flow symmetry in the nozzle should be mentioned.

A temperature traverse 28 inches from the fuel injector (12 in. upstream of the nozzle throat) yielded a temperature spread of less than 360 Fahrenheit degrees at an equivalence ratio of 0.364 (fig. 14). A flatter profile would be expected at the combustor exit and throughout the nozzle. When an abrupt condensation step occurred (see Abrupt Condensation Phenomena in this section), it was sensed by each of the pressure taps at a given station. The sensing of a small, yet well-defined, abrupt condensation step by each of these taps implies that the flow was symmetrical about the longitudinal axis of the nozzle. Also, pressure data (figs. 15(a) and (b)) at the stations prior to abrupt condensation indicate that the flow was expanding along the one-dimensional flow path. These observations, taken together, indicate that an orderly, though not necessarily uniform, flow field existed.

Behavior of Liquid Boric Oxide in Nozzle

If the velocity and temperature of the boric oxide particles lag relative to the other products during expansion, a thrust loss will occur. At an equivalence ratio of 0.35, the combustion products of a pentaborane flame contain 7 percent by weight boric oxide. The enthalpy of the oxide is 15 percent of the enthalpy of the other products combined. In fact, air

specific impulse can be reduced as much as 5 percent if the liquid does not exchange momentum and heat with the other products. This large thrust loss would occur only if the oxide particles were very large; reference 7 shows that the thrust loss will be negligible, provided the particles have a diameter of less than 3 microns. Extrapolation of the particle-size studies of reference 8 to the conditions tested indicates that the liquid oxide particles would be much smaller than 3 microns in diameter.

The experimental results can be used in several differing ways to show that the liquid particles were very small and in temperature and velocity equilibrium with the gas stream during the expansion process. These results are based on data obtained at equivalence ratios of 0.318 and 0.364, where the boric oxide remained entirely in the liquid phase throughout the nozzle. Thrust data show that the average deviation of the experimental thrust from the ideal thrust is 0.8 percent (derived from data points given in figs. 16 and 17) at both the throat and the exit of the nozzle. Therefore, no discernable thrust loss occurred in the nozzle when the boric oxide was in the liquid phase. (Appendix D can be used to show that the test results are not in error because of the assumed subsonic equilibrium expansion that was used in the data calculation procedure.)

A somewhat more sensitive method of determining the extent to which the liquid oxide particles depart from temperature and velocity equilibrium can be illustrated by means of figures 15(a) and 18. In the nozzle divergence, a nonequilibrium expansion would yield lower static-pressure ratios p/P_4 than would result from an equilibrium expansion. Figure 15(a) shows that the pentaborane data and the calibration data were in very close agreement at nozzle stations 4 to 11. The slight deviation from the calibration curve past station 11 is within experimental data scatter (appendix B). Also, the divergence efficiency (fig. 18), which is based on the pressure measurements, shows that the particle-laden gas stream has practically the same divergence efficiency as shown by the calibration data.

The foregoing observations can be summarized as follows: When the boric oxide was all in the liquid phase, the expansion process showed that the liquid particles were, for all practical purposes, in thermal and velocity equilibrium with the rest of the products.

Abrupt Condensation Phenomena

During an equilibrium expansion process, vapor begins to condense when the partial pressure of the vapor reaches the saturation pressure. These two pressures remain the same throughout the rest of the expansion.

[REDACTED]

However, if the expansion process occurs suddenly, condensation may not have time to occur in a nozzle. In this case, the vapor becomes supercooled; that is, the vapor pressure becomes greater than the saturation pressure. Expansion without phase change is defined herein as a frozen expansion process. (The ideal performance data of figs. 16 and 17 were calculated for frozen expansion processes.)

In actual practice, a frozen expansion process of a supercooled vapor does not continue indefinitely. For example, many studies of the expansion of water vapor show that a point in the expansion process is eventually reached where condensation occurs. Condensation occurring in this manner manifests itself by a sudden change in the static pressure, which is easily measured experimentally. In the case of steam, a rapid condensation process proceeds until a condition of (or near) liquid-vapor equilibrium is reached. In the experiments reported in reference 9, the rapid condensation step occurred in the nozzle divergence and required a distance of 0.3 inch. Following the sudden adjustment in phase, the remainder of the expansion process occurred at near equilibrium conditions. In this report, the rapidly occurring condensation of supercooled vapor is called an abrupt condensation step.

Abrupt condensation was observed in the convergent portion of the nozzle at equivalence ratios of 0.482, 0.535, and 0.577 (fig. 15(b)). Since the pressure taps were not spaced closely enough to define the curve within the region of condensation, wide broken curves were faired through this region. At the two leaner equivalence ratios (0.482 and 0.535), this condensation took place between stations 6 and 7. At the higher equivalence ratio (0.577), the condensation step occurred between stations 7 and 8. The abrupt condensation step was observed as a relatively sudden decrease (4 to 7 percent) in the static-pressure ratio p/p_4 . Before and after the interval when abrupt condensation occurred, the pressure-ratio-data curves have almost the same slope as the curves for no phase change.

The extent to which the products deviate from phase equilibrium will be discussed when these data are compared to an equilibrium expansion process. The amount of condensation that occurs in the nozzle and the effect of this condensation on the accuracy of the calculated results of table III are discussed in the following paragraph.

The influence coefficients given by Shapiro (ref. 10) were used to determine the amount of vapor that suddenly condensed. The basic equation is:

$$\frac{(\Delta p)'}{p'} = - \frac{\gamma (M')^2}{1 - (M')^2} \left[\frac{(\Delta w_L)' h_v}{H_p' w_p} - \frac{(\Delta R)'}{R'} \right]$$

where a symbol bearing a prime represents the mean value of the property at the location of phase change; and the symbols $(\Delta p)'$, $(\Delta w_1)'$, and $(\Delta R)'$ represent the change in value of the property resulting from a phase change. Equation (8) relates w_1 to R . The results are given in table IV. For a given change in vapor content, the change in the other fluid properties was readily computed. Not over 4 percent of the total boric oxide present condensed abruptly at an equivalence ratio of 0.577. At the two leaner equivalence ratios, the amount of the condensing oxide was between 8 and 16 percent of the total boric oxide present. The probable error in the amount of oxide that changes phase during the step is about 100 percent. The probable error in the change of the other fluid properties given in table IV is of a similar magnitude. This unfortunate circumstance arose because the $(1 - (M')^2)$ term in the equations vanishes as M' , the Mach number at the time of condensation, approaches unity.

The fact that the pressure drop in the condensation step was somewhat greater at an equivalence ratio of 0.535 than at 0.482 does not imply a greater phase change. The possibility exists that condensation at the leaner equivalence ratio may have occurred at a slightly lower Mach number and thus yielded an increased amount of phase change for a given pressure defect.

The pentaborane data curves (fig. 15) have nearly the same slope as the calibration data curves in all cases except the three instances where abrupt condensation occurred. Had the slopes been slightly steeper before the throat or slightly flatter after the throat, a gradual condensation process would have existed. Since this was not the case, a frozen expansion process, prior to and after a small, abrupt phase change, existed at equivalence ratios of 0.482, 0.535, and 0.577.

The effect of the observed condensation on the methods presented for computing performance was sufficiently small that inclusion in the ANALYTIC PROCEDURE section was not warranted. Table IV shows the total-pressure loss resulting from the condensation steps. Had corrections for these losses been incorporated in the calculation procedure used to compute table III, then (1) the combustion-efficiency values at an equivalence ratio of 0.577 would have been approximately 1 percent lower, and (2) the boric oxide that existed in the condensed phase at the nozzle throat for equivalence ratios of 0.482 and 0.535 would have been decreased by as much as 15 percentage points. Appendix D shows that the stream-thrust values F_g computed by means of the calculation procedure differ only slightly from F_g values that incorporate a correction for the condensation step.

The fraction of condensed oxide (tables III and IV) provides a means of estimating the fraction of oxide in each phase prior to the abrupt condensation step. These estimates stress the possibility that a mixed



phase existed prior to the condensation step. At an equivalence ratio of 0.482, the estimate shows that some liquid is present, even though the data are adjusted so that the maximum experimental error is used to increase the amount of vapor present.


Effect of Abrupt Condensation on Performance

4533 In general, analytical studies show that condensation of the boric oxide in an engine is beneficial. For a given engine, at a given set of air and fuel flows, condensation has the following effects on thrust: Phase change in the combustor or nozzle convergence results in a higher system pressure, and phase change in the nozzle divergence produces greater pressure on the divergent surfaces. In both cases, thrust is increased. The greater the amount of condensation and the lower the Mach number during the condensation process, the greater will be the thrust increase due to condensation. Figure 16 shows that, for an equivalence ratio of 0.45, the ideal air specific impulse is increased from 137 to 147 seconds when the boric oxide is completely condensed in the combustor. This thrust increase can be interpreted as the result of an increase in system pressure for a given engine configuration and for given flow rates.

A comparison of the ideal and the experimental data for equivalence ratios of 0.482 and 0.535 in figure 16 shows that the air-specific-impulse values are appreciably greater than would have been the case for an all-vapor expansion process. Even a small thrust benefit is indicated when (equivalence ratio, 0.577) only a small amount of the oxide is condensed.

The air specific stream thrusts (fig. 17) for the tests at equivalence ratios of 0.482 and 0.535 were higher than the ideal performance for all of the boric oxide in the vapor phase. The static-pressure taps showed that condensation of the oxide occurred in the convergent, but not in the divergent, part of the nozzle. Condensation of boric oxide in the combustor and in the convergent part of the nozzle would be expected to increase the total pressure of the system and thus increase the momentum of the expanding stream. However, it is conceivable that under certain conditions an abrupt condensation step near the throat could result in a lowering of air specific stream thrust. This phenomenon was believed to have occurred at an equivalence ratio of 0.577 (see fig. 17), although the accuracy of the data is not sufficient to prove this point. A possible explanation follows.

The criterion used in this report to measure the effectiveness of the nozzle divergence is nozzle divergence efficiency. Both the numerator and denominator of the divergence efficiency equation

$$\eta_w = \left(\frac{\sum pA}{\Delta F_{id}} \right) 100$$


are based on the same stagnation pressure P_4 . For a constant value of P_4 , condensation occurring in the convergence yields a static-pressure drop that, in turn, lowers the pressure on the walls of the divergent section and lowers the value of η_w . Figure 18 shows that η_w decreased from 80 to 69 percent when an abrupt condensation step occurred. This phenomenon could explain the stream-thrust (F_{15}) observation of a lower air specific stream thrust than the ideal all-vapor calculation predicts at an equivalence ratio of 0.577.

Comparison of Experimental Results with Several Ideal Models

The experimental results are compared with the ideal analytical results for the following conditions:

- (1) Essentially all the boric oxide is in the liquid phase throughout the expansion.
- (2) All the boric oxide is in the vapor phase during the expansion.
- (3) The boric oxide is in phase equilibrium at the combustor exit and remains so throughout the expansion.
- (4) The boric oxide is in phase equilibrium at the combustor exit, but no further phase change occurs during the expansion (frozen).

Three comparisons of the ideal and experimental results are shown in figures 19, 20, and 21 for the combustor-exit station, the nozzle-throat station, and the nozzle-exit station, respectively. The experimental results presented in figures 20 and 21 were obtained from table III. The experimental data of figure 19 were obtained in the following manner: The analysis showed that, at equivalence ratios of 0.482 and 0.535, approximately 10 percent of the boric oxide condensed in the nozzle convergence and, at an equivalence ratio of 0.577, 4 percent of the oxide condensed. By using these values, the combustor-exit temperature $T_{4,corr}$ was computed from equation (5c):

$$T_{4,corr} = T_{8,corr} - \Delta T = \frac{t_{8,corr}(r_8 + 1)}{2} - \Delta T$$

where $t_{8,corr}$ (calculated from eq. (27)) is obtained from table III, and ΔT is the temperature rise resulting from the condensation step.


The ideal data for figures 19 to 21 were obtained from analytical models that differed only in the behavior of the boric oxide. The ideal all-liquid and all-vapor models have been described previously. The ideal

equilibrium-phase model is based on the boric oxide vapor-pressure data shown in figure 22. The ideal data for figures 20 and 21 include a fourth model which assumes that the boric oxide is in phase equilibrium at the combustor exit but that it expands without a further change in phase. All the ideal models shown in figure 21 recognize the thrust loss resulting from three-dimensional flow in the nozzle divergence (see eq. (30)).

At the combustor exit, the ideal equilibrium data show that vaporization begins at about 3300° R and is completed at about 4000° R (fig. 19). The experimental data agree closely with the equilibrium data up to 3300° R; however, when the oxide begins to vaporize, the experimental curve breaks away from the ideal equilibrium curve. For example, the experimental data show that none of the boric oxide has condensed at an equivalence ratio of 0.58, whereas the ideal equilibrium data show that one-half of the oxide should have condensed. At this equivalence ratio, the experimentally determined combustion temperature was 3600° R, or about 400 Fahrenheit degrees lower than the temperature where the ideal equilibrium data show that the oxide has entered an all-vapor state. However, the experimental results and the ideal all-vapor data were identical at equivalence ratios above 0.58. Therefore, the ideal and experimental data are in good agreement, except that the transition from a liquid phase to a vapor phase occurs at a lower temperature than the ideal model predicts. The reason cannot be determined from the data; however, several possible reasons are proposed: (1) An equilibrium condition may not have existed downstream of the primary combustion zone of the combustor; (2) an error may have existed in the vapor-pressure data; (3) a boron compound other than boric oxide (B_2O_3) may have been present; and (4) deviations existed between the experimentally obtained flow and the ideal uniform flow. Item (1) is based on the previously discussed observation that the boric oxide vapor appeared very reluctant to condense in the nozzle even when some liquid was present. This observation is all the more interesting, since the combustor had an unusually long dwell time and a high degree of turbulence and thereby afforded a good environment for the attainment of equilibrium. Each of the foregoing reasons for the discrepancy between the ideal and experimental data is expected to apply to full-scale engines.

The results shown for performance at the nozzle throat (fig. 20) are roughly parallel to the results shown for the combustor-exit station. For example, the figure shows that, in the region where the oxide was in the all-vapor or all-liquid phase, the experimental data are in good agreement with the ideal data.

For any boron-containing fuel, there exists a point on the curve of impulse against fuel-air ratio where an increase in fuel-air ratio causes an appreciable amount of boric oxide to vaporize. This threshold point marks the beginning of the region where the specific fuel consumption



increases rapidly for an increase in thrust level. When the equivalence ratio is in the vicinity of 0.55, the experimental data (fig. 21) show that an 8-percent increase in fuel consumption is required to obtain a 1-percent thrust improvement. This effect is less pronounced at all other equivalence ratios investigated. By defining the threshold point as the place where 20 percent of the boric oxide is in a vaporized state, the threshold point for the experimental data (fig. 20) occurs at an equivalence ratio of 0.45. The corresponding threshold point for the ideal equilibrium expansion data is at an equivalence ratio of 0.56. On this basis, the threshold point occurs when the combustor temperatures (fig. 19) are 3400° and 3880° R for the experimental data and the ideal equilibrium expansion data, respectively.

The results obtained at the nozzle exit (fig. 21) are very similar to those obtained at the throat station. At equivalence ratios outside the region where the oxide is changing phase, the experimental data fit the ideal data curves. In the region of phase change, the experimental data are farther from the ideal equilibrium expansion curve since no condensation of the oxide occurred in the divergence. For instance, the experimental specific thrust at an equivalence ratio of 0.58 is 6 and 5 percent below the equilibrium specific thrust curve at the nozzle-exit and nozzle-throat stations, respectively. However, an inspection of the ideal thrust data (figs. 20 and 21) shows that only a very small thrust benefit is obtained from an equilibrium expansion (in contrast to a frozen expansion) in the nozzle divergence alone.

Figure 21 illustrates the maximum extent to which the experimental data departed from the ideal equilibrium predictions. For example, the greatest deviation is found at an air specific stream thrust of 167 seconds, where the analytical data predict that nearly all the oxide should be in the liquid phase, while the experimental data show that nearly all the oxide is still in the vapor phase. The actual equivalence ratio is 0.577, and the ideal equivalence ratio is 0.480. This means that the actual fuel consumption is 20 percent higher than that calculated for ideal equilibrium data. This departure may be extremely significant for an actual engine when performance is calculated from theoretical vapor-pressure data.

Effect of Oxide Films

Inspection of the apparatus after each run revealed rough boric oxide films on the surfaces exposed to the combustion products; however, these solid deposits were of little value in estimating the film thickness and surface texture that existed during the test. Fortunately, the data that were obtained during each test did provide a means of measuring the thickness and frictional effect of the liquid films on the nozzle surfaces.

Boric oxide can accumulate on a given surface in several ways. At high temperatures, condensation of the oxide vapor on the cooler surfaces is to be expected. Chunks of oxide, which are above the solidification point (about 800°F for B_2O_3), can be blown from one surface to another. However, one of the most common and best understood forms of deposition is due to the diffusion of minute liquid particles from an oxide-laden stream. The deposition-rate equations of reference 11 for the diffusion of liquid particles to a surface were used to determine the deposition rate at a flame temperature of 2800°R . Results, presented in figure 23, show that 0.04 inch of film could form in 60 seconds of running time for pentaborane fuel. At oxide film temperatures above the solidification point, the film will start to flow along the surface because of the dynamic force of the gas stream. Reference 12 presents a detailed analysis of this liquid flow. After sufficient time has elapsed, the removal rate equals the collection rate, and an equilibrium film thickness is reached. This thickness is largely dependent on the oxide viscosity, which is very great at the temperature of interest (see fig. 24).

The experimental data (fig. 23) were determined as follows: Complete combustion of the pentaborane and the existence of an all-liquid boric oxide phase were assumed. These assumptions, together with equations (7) to (10), provided a means of computing the open area (effective A_n) at the throat. The ratio of the computed area to A_n is the ordinate scale shown in the figure. The 940°F wall-temperature data were obtained from runs 1 and 3a, which are presented in tables I to III. The data obtained at the lower temperatures were considered suitable only for a study of films.

As a whole, the experimental data in figure 23 indicate that less than 40 seconds of running time were sufficient to attain an equilibrium film thickness at the throat. The surface temperature of the throat wall rose from a value of about 500°F at the start of pentaborane flow to the value shown at the time the data points were taken. The higher wall temperatures were associated with the higher combustor temperature data. Figure 23 indicates that, when the throat-wall temperatures were above 1000°F , the oxide films would be very thin and would reduce the throat area of a 4-inch-diameter nozzle by a very small amount.

Nozzle-wall temperatures and temperature gradients were lower on the divergent surface than on the throat surface; hence, thicker oxide films can be expected on the divergent surfaces. Other investigators have shown that the surface of a thick flowing film can become very uneven because of the wave-like motion of the flow. Thus, the accompanying frictional losses could be large. The friction data given in figure 25 support this viewpoint. A description of the calculation procedure used to obtain these friction data follows. By disregarding the experimental errors involved in measuring $F_{15,bb1}$, the thrust barrel yields the true thrust

of the nozzle. The amount of thrust loss resulting from the oxide films in the nozzle can be determined by comparing $F_{15,bb}$ with F_{15} from equation (23); however, this thrust loss is a combination of several factors, namely, nozzle-throat-area change, friction on the divergent surfaces, and friction on the convergent surfaces. Therefore, equation (23) is adjusted as follows: Friction on the convergent surfaces, relative to friction on the divergent surfaces, is small and can be neglected for the purpose of this discussion. A small correction, as indicated in figure 23, is required in order to reduce the F_{15} values because of the presence of a smaller throat area than that provided by equation (23). The loss in stream thrust (in percent) then becomes

$$\left[\frac{F_{15} \left(\frac{A_{n, \text{effective}}}{A_n} \right) - F_{15,bb}}{F_{15,bb}} \right] 100$$

and is a measure of the frictional resistance experienced in the nozzle divergence. Although the data accuracy is poor, trends can be obtained from the results. Figure 25 shows that friction increased as soon as the film began to grow but that, after about 10 seconds, the frictional loss began to decrease. At the lower equivalence ratios investigated, an equilibrium condition was not reached at the end of the test. At this time, stream-thrust loss due to friction was observed to be in the vicinity of 3 percent. At the highest equivalence ratio, the wall temperature for most of the divergent surface quickly rose above the solidification point of the oxide, and a constant friction loss was established within 30 seconds of running time. In this case the steady-state friction loss was too small to measure.

The minimum wall temperature at which an oxide-produced friction loss becomes objectionable cannot be obtained from these data because of poor data accuracy and large axial-temperature gradients on the nozzle surface. However, a temperature at which friction loss, as measured, was not objectionable can be obtained from figure 25. For a midpoint (station 11) temperature of approximately 800°F , the data as a whole indicate that the friction loss was too small to be measured by the apparatus. Since a portion of the surface downstream of the midpoint was at a considerably lower temperature, a nozzle operating at a stagnation temperature above 2800°R and a wall temperature above 800°F is not expected to suffer objectionable friction losses. At nozzle-wall temperatures in the region of 600°F , a loss of several percent in stream thrust is indicated.

The results of the oxide-film studies can be used to explain an anomaly existing in the tabulated data. At the two lowest equivalence ratios investigated, nozzle-wall temperatures were conducive to deposit formation. The method used to compute combustion efficiency omitted any



adjustment for an oxide film in the nozzle throat; if the throat area had been reduced to allow for this film, computed efficiency would have been lower. For example, a reduction of 1 percent in the nozzle-throat area results in a 2.5-percent decrease in the computed combustion efficiency at equivalence ratios of 0.3 to 0.4. The existence of a moderately thick oxide film could be used to explain why the combustion-efficiency data (table III) are several percent above the ideal value. However, combustion-efficiency data were not adjusted for the effect of a film for two rather obvious reasons: First, these two data points were used in presenting part of the story on the oxide-film thickness and, second, any adjustment would be well within the limits of experimental error.

SUMMARY OF RESULTS

A study of the behavior of pentaborane-air combustion products flowing through a 7-inch-long convergent-divergent nozzle gave the following results. (Similar results could be expected in full-scale engines, because the test combustor provided unusually long residence times and a highly turbulent environment.)

1. The experimentally determined thrust and specific fuel consumption agreed with the ideal performance for completely condensed boric oxide at combustor-exit total temperatures up to 3300° R. For all practical purposes, the liquid is in thermal and velocity equilibrium with the rest of the combustion products.

2. The experimentally determined thrust and specific fuel consumption agreed with the ideal performance for completely vaporized boric oxide at combustor-exit total temperatures greater than 3600° R. Complete vaporization of the oxide was observed at temperatures about 400 Fahrenheit degrees less than predicted by ideal analysis. Between 3600° and 4000° R, specific fuel consumption was as much as 20 percent greater than predicted by an ideal equilibrium expansion process.

3. Between 3300° and 3600° R, experimentally determined thrust and specific fuel consumption were between those values predicted by assuming completely condensed boric oxide and completely vaporized oxide.

4. Within the nozzle, condensation of the oxide was observed only in the convergence and only in the form of an abrupt step. The amount of oxide condensed was considerably less than that indicated by an equilibrium expansion process. This abruptness of condensation was observed even when liquid boric oxide was present at the nozzle inlet.

5. In one test, abrupt condensation of the boric oxide immediately upstream of the nozzle throat appeared to result in a small thrust loss rather than the small thrust gain that is usually expected to accompany



a condensation process. The observed loss stemmed from an appreciable lowering of static pressure on the divergent surface of the nozzle.

6. Oxide films on the nozzle surfaces were found to increase greatly the frictional losses in the divergence and to reduce the throat flow area. The effect of liquid boric oxide films was negligible when the throat-wall temperatures and the divergence-wall temperatures were maintained above 1000° and 800° F, respectively. With nozzle walls below this temperature, as much as 6-percent loss in stream thrust was observed because of the combined effect of wall friction and reduced throat area.

7. A computational method for separating performance losses due to combustion inefficiency from performance losses due to lack of phase equilibrium was developed. This method avoids the use of boric oxide vapor-pressure data but does require experimental data for both all-liquid and all-vapor expansion up to the nozzle throat.

8. Combustion efficiencies were calculated to be 100 percent over the range of equivalence ratios tested (0.32 to 0.64). These high efficiencies were associated with high pressure losses across the fuel injector.

Lewis Flight Propulsion Laboratory
National Advisory Committee for Aeronautics
Cleveland, Ohio, October 7, 1957

APPENDIX A

SYMBOLS

A	area, sq in.
A_n	cross-sectional area of nozzle throat at 70° F
a	speed of sound, ft/sec
C_d	coefficient of discharge
C_{fr}	coefficient of friction
C_k	thermal-contraction coefficient
C_m	momentum coefficient
C_p	molar specific heat at constant pressure, Btu/(lb-mole)(°R)
c_p	weight specific heat at constant pressure, Btu/(lb)(°R)
F	stream thrust, lb
ΔF	actual thrust change between nozzle throat and exit, lb $\Delta F = F_{15} - F_8 = \Sigma pA - \text{friction}$
ΔF_{id}	thrust change between nozzle throat and exit for one-dimensional isentropic flow of an ideal gas
f/a	fuel-air ratio
g	gravitational constant, 32.17 ft/sec ²
H	enthalpy per pound of air, Btu/lb
h_c	heat of combustion, Btu/lb
h_v	heat of vaporization of boric oxide, Btu/lb
k	constant dependent on nozzle geometry
M	Mach number
n	number of moles
P	total pressure, lb/sq in. abs

4533

- p static pressure, lb/sq in. abs
- ΣpA pressure force on divergent area of nozzle obtained by graphical integration of wall static pressure against cross-sectional area, lb
- Q heat rejected to coolant, Btu/sec
- R fluid constant, ft-lb/(lb mixture)(°R)
- S_a air specific impulse, lb stream thrust/(lb air)(sec)
- T total temperature, °R
- t static temperature, °R
- V velocity, ft/sec
- w weight flow rate, lb/sec
- Y^* factor of continuity equation,
$$\sqrt{\frac{\gamma g}{\left(\frac{\gamma + 1}{2}\right)^{\frac{\gamma + 1}{\gamma - 1}}}}$$
- Z^* factor of momentum equation,
$$2^{\frac{\gamma}{\gamma - 1}}(\gamma + 1)^{\frac{1}{1 - \gamma}}$$
- γ ratio of specific heats
- η_c combustion efficiency
- η_w divergence efficiency, $(\Sigma pA/\Delta F_{id})100$
- ρ density, lb/cu ft
- ϕ equivalence ratio

Subscripts:

- a air
- bb1 barrel
- corr corrected
- f fuel

g gaseous

id ideal

l liquid

t total

v vapor

Numerical subscripts denote axial position (figs. 1 and 2); specifically,

2 upstream of fuel injector

3 downstream of fuel injector (prior to combustion)

4 combustor exit

8 nozzle throat

15 nozzle exit



APPENDIX B

ACCURACY OF EXPERIMENTAL RESULTS

The statements presented in this appendix are based on an over-all analysis of not only the data in the present report but also an approximately equal amount of supplemental data. The estimates given are based, whenever possible, on independent methods of measurement. The accuracy limits, when not obtained by independent measurements, are based on the authors' best judgment of the data.

Air- and fuel-flow rates were measured with an estimated error of 1 percent. Except when oxide films were either very thick or very viscous, the static-pressure data for stations 4 to 14 were unaffected by the oxide; nozzle pressure data became less accurate as the absolute value of pressure decreased. Whereas pressure data obtained at stations 4 to 8 appeared to have an error of no more than 0.5 percent, an error several times larger existed in the region of stations 9 to 11. A 5- to 10-percent error existed at stations 13 and 14; this error is attributed primarily to water that condensed in the pressure lines.

Errors in the computed values of C_d and C_m were considered negligible. These coefficients depended primarily on the curvature of the nozzle. For the geometry of the test nozzle, a wall Mach number of 1.08 was theoretically predicted for the throat station. Figure 13 shows that the wall Mach number, determined from the calibration data, was very close to the predicted value.

Several calibration tests in which total-pressure measurements were taken at the nozzle exit showed that no discernible loss occurred in the total pressure between the nozzle entrance and exit.

The over-all precision and accuracy of the results obtained from equation (7), upon which the combustion-efficiency computations are based, can be demonstrated by means of figure 10. The average data scatter of the C_k values is less than 0.5 percent. The experimentally determined curve, which should pass through unity at a temperature of 70° F, is in error by 0.4 percent at this temperature. These results were obtained at operating conditions comparable to those for pentaborane. When equation (7) is used to calculate T_8 for pentaborane data, all the experimentally determined terms in the equation are squared; this results in an estimated 2-percent error in T_8 values. This 2-percent error in temperature is reflected as a 2.5- to 3-percent error in combustion efficiency (eq. (10)). Both errors are based on the absence of oxide films thick enough to reduce the throat area.

CONFIDENTIAL

Divergence efficiency values were observed to be reproducible within 3-percent limits; accuracy of the values is considered to be of a similar proportion. This error will affect the thrust, equation (23), by no more than 0.3 percent.

Thrust values F_8 and F_{15} are believed to be accurate to within ± 1 percent in the absence of appreciable oxide films. Stream-thrust ($F_{15,bb}$) values obtained with the thrust barrel lacked the degree of accuracy cited for the other thrust determinations. The $F_{15,bb}$ data are judged to contain a possible error of 2 to 3 percent for all the tests presented in the report.

4533

CN-5

[REDACTED]

APPENDIX C

COMBUSTION EFFICIENCY

The ANALYSIS OF RESULTS shows that the presence of oxide films and abrupt condensation steps had a noticeable effect on certain aspects of performance. The discussion also shows that the combustion-efficiency values (table III) would have been different if proper corrections had been made for these phenomena. For any of the tabulated tests, the combination of these corrections was less than the experimental error arising from the data used to calculate the combustion efficiencies. The experimental error, itself, was estimated to be less than 3 percent. This error was based on the premise (stated in the ANALYTIC PROCEDURE) that combustion efficiencies would be calculated by assuming that:

- (1) At the lowest equivalence ratios, 0.318 and 0.364, the boric oxide was essentially in an all-liquid phase at the nozzle throat.
- (2) At the highest equivalence ratio, 0.639, the boric oxide was in an all-vapor phase at the nozzle throat.

The validity of these two assumptions is proved in the following discussion. Proof of either assumption is not forthcoming from an inspection of any one piece of data because of the magnitude of the previously mentioned experimental error. Proof of the existence of a known phase at the throat cannot be based solely upon any singular result, but rather on a combination of circumstances.

The following gives proof that the boric oxide was essentially all liquid at the two lowest equivalence ratios investigated. Table III shows that the computed combustion efficiencies were 101.1 and 102.6 percent at equivalence ratios of 0.318 and 0.364, respectively. An assumption that some of the oxide was vapor instead of liquid would yield even higher efficiency values, whereas an excuse to lower the values is needed. Second, figure 22 shows that the boric oxide vapor pressure at the combustor-exit temperature was less than 0.002 atmosphere in both tests. This pressure, at equilibrium conditions, would permit less than 2 percent of the oxide to exist as a vapor. Upon expansion in the convergence, the vapor would tend to condense. The conclusion therefore is drawn that the boric oxide was in an all-liquid phase at the nozzle throat. (Combustion efficiency values above 100 percent are a result of experimental error due largely to the existence of the liquid oxide film that reduced the nozzle-throat area.)

In order to prove that the boric oxide at the throat was in an all-vapor state at the highest equivalence ratio tested (0.639), seven observations, some of which are absolutely independent of each other, are listed:

DECLASSIFIED

(1) Measurements indicated that, if the oxide were all vapor, the combustion efficiency was 100 percent. If liquid oxide was present, a lower efficiency would have been calculated.

(2) Samples of combustion products showed combustion efficiency to be very near 100 percent.

(3) At the time when the oxide was assumed to be completely vaporized, the computed combustion efficiency was 99.9 percent. If liquid had actually been present, the assumption of complete vaporization would yield a higher-than-actual combustion efficiency. Thus, it is possible for the presence of a small amount of liquid to balance an actual combustion inefficiency. However, such an exact balance is considered unlikely in view of the other evidence presented.

(4) The boric oxide was 96-percent vaporized at a lower equivalence ratio (0.577), as calculated when 100-percent combustion efficiency was assumed. Observations indicate that the fraction vaporized should increase with increasing equivalence ratio. On this basis, the oxide should be completely vaporized at an equivalence ratio of 0.639.

(5) Item (4) can be substantiated by a further bit of evidence: In the abrupt condensation step at equivalence ratio 0.577, less than 4 percent of the oxide was calculated to have condensed. This agrees with the 96-percent vaporization calculated when 100-percent combustion efficiency was assumed.

(6) If a loss in combustion efficiency is assumed to compensate exactly for the presence of liquid oxide at both 0.577 and 0.639 equivalence ratios, the combustion efficiency would be higher at the higher equivalence ratio. This trend would be contrary to that observed in this program (with fuel injector A) and in other programs.

(7) The nozzle static-pressure data did not indicate any change in phase (in the nozzle) for the 0.639 equivalence ratio.

These arguments, when combined, show that all the oxide was in the vapor phase at the nozzle throat for the highest equivalence ratio investigated. The arguments also show that the oxide was very nearly all vaporized at the throat for an equivalence ratio of 0.577. Hence, the abrupt condensation step at the latter test condition was from an all-vapor to a mixed phase; this is the customary form of a condensation step observed for water vapor.

The conclusions reached in this discussion confirm the calculation of combustion-efficiency values very near 100 percent at the two leanest equivalence ratios and the two highest equivalence ratios tested. At the

4533

CN-5 back

03:41:00 [REDACTED] 03:00

two intermediate equivalence ratios (0.482 and 0.535), no accurate direct method is available for computing combustion efficiency; however, no indication of a reduction in performance was observed. On the basis of these observations, the combustion efficiency for each test of table III was, for all practical purposes, concluded to be 100 percent.

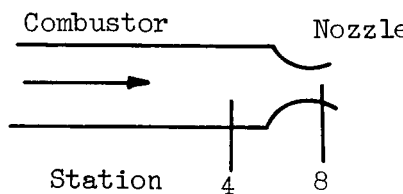
[REDACTED]

APPENDIX D

ERRORS IN THRUST COMPUTATIONS DUE TO NON-IDEAL EXPANSION
IN NOZZLE CONVERGENCE

A method of computing the thrust at the nozzle throat F_8 for non-ideal subsonic expansion processes is presented in this appendix. Moreover, an example shows the error involved when equation (13) of the ANALYTIC PROCEDURE is used to determine F_8 for an abrupt condensation step.

From the diagram,



$$F_4 = p_4 A_4 (1 + \gamma M_4^2) \quad (11a)$$

where $\gamma M_4^2 \approx 0.02$ for the test nozzle. Since P_4 is approximately equal to $1.01 p_4$, it follows that

$$F_4 = k P_4$$

where k is a constant primarily dependent on the geometry of the nozzle.

The stream thrust at the nozzle throat can be expressed as

$$F_8 = F_4 - \int_{A_8}^{A_4} p \, dA = k P_4 - \int_{A_8}^{A_4} p \, dA \quad (D1)$$

The integral can be evaluated in the manner described in the ANALYTIC PROCEDURE. This equation is applicable regardless of the nature of the expansion process; however, for the purposes of the argument presented, (D1) is restricted to the case of non-ideal expansion of pentaborane products of combustion.

A parallel equation,

$$F'_8 = F'_4 - \left(\int_{A_8}^{A_4} p \, dA \right)' = kP'_4 - \left(\int_{A_8}^{A_4} p \, dA \right)' \quad (D2)$$

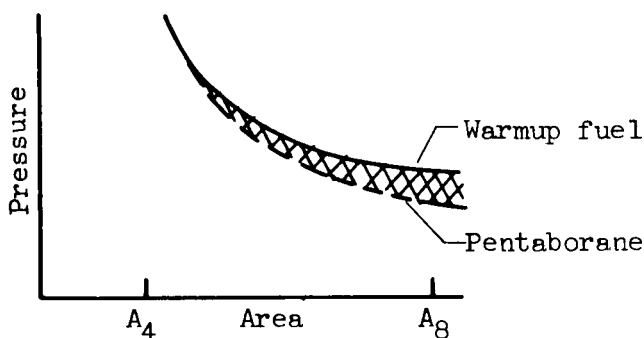
expresses the behavior of the calibration data.

Consider that a calibration test and a pentaborane test were conducted at the same total pressure P_4 . The constant k is independent of the fuel type, provided γ is not widely different for the two tests. Also, F'_8 is accurately obtained from equation (13). By subtracting equation (D1) from (D2), the stream thrust of the pentaborane products becomes

$$F_8 = F'_8 - \int_{A_8}^{A_4} p \, dA + \left(\int_{A_8}^{A_4} p \, dA \right)' \quad (D3)$$

The absolute value of each of the integrated quantities is much larger than F_8 . Hence, a large error in F_8 can result from an attempt to evaluate the integral.

This error can be avoided by use of the following procedure. The pressure data from the two tests can be presented on a graph:



The cross-hatched area represents the quantity $-\int_{A_8}^{A_4} p \, dA + \left(\int_{A_8}^{A_4} p \, dA \right)'$, and measurement of the area determines the force that must be added to F'_8 in order to obtain F_8 .



At equivalence ratios of 0.482, 0.535, and 0.577, the abrupt condensation steps caused the pressure-area curves to depart from the curve obtained with the warmup fuel. The greatest departure occurred at an equivalence ratio of 0.535 (fig. 15(b)). For this test, the defect represented by the cross-hatched area corresponds to 0.005 Fg. Therefore, the air-specific-impulse values computed from equation (13) are 1/2 percent lower than the actual impulse. Since the error was so small, the data of table III were not corrected for the observed non-ideal flow behavior in the nozzle convergence.

REFERENCES

1. Tower, Leonard K.: Analytic Evaluation of Effect of Inlet-Air Temperature and Combustion Pressure on Combustion Performance of Boron Slurries and Blends of Pentaborane in Octene-1. Supplement 1 - Influence of New Boric-Oxide Vapor-Pressure Data on Calculated Performance of Pentaborane. NACA RM E56D02, 1956.
2. Setze, Paul C.: A Review of the Physical and Thermodynamic Properties of Boric Oxide. NACA RM E57B14, 1957.
3. Glawe, George E., Simmons, Frederick S., and Stickney, Truman M.: Radiation and Recovery Corrections and Time Constants of Several Chromel-Alumel Thermocouple Probes in High-Temperature, High-Velocity Gas Streams. NACA TN 3766, 1956.
4. Streiff, M. L.: Exit-Nozzle Design. APL/JHU TG 154-13, ch. 13 of Ramjet Technology, Appl. Phys. Lab., The Johns Hopkins Univ., 1953. (Contract NOrd 7386 with Bur. Ord., Dept. Navy.)
5. Fivel, Herschel J., Tower, Leonard K., and Gibbs, James B.: Pentaborane Combustion Performance in 9.75-Inch-Diameter Ram-Jet Engine in Connected-Pipe Altitude Facility. NACA RM E54I16, 1957.
6. Eckert, E. R. G.: Engineering Relations for Friction and Heat Transfer to Surfaces in High Velocity Flow. Jour. Aero. Sci., vol. 22, no. 8, Aug. 1955, pp. 585-586.
7. Barry, F. W.: Performance of a Ramjet Burning Pentaborane - Effect of Liquid Droplets in Exhaust Nozzle. Rep. AL-1712, Missile and Control Equip., North Am. Aviation, Inc., Oct. 28, 1953.
8. Setze, Paul C.: A Study of Liquid Boric Oxide Particle Growth Rates in a Gas Stream from a Simulated Jet-Engine Combustor. NACA RM E55I20a, 1957.



03712 ~~CONFIDENTIAL~~ 30

9. Binnie, A. M., and Woods, M. W.: The Pressure Distribution in a Convergent-Divergent Steam Nozzle. Proc. Inst. Mech. Eng., vol. 138, Jan.-May 1938, pp. 229-266.
10. Shapiro, Ascher H.: The Dynamics and Thermodynamics of Compressible Fluid Flow. Vol. I. The Ronald Press Co., 1953.
11. Setze, Paul C.: A Theoretical and Experimental Study of Boric Oxide Deposition on a Surface Immersed in an Exhaust Gas Stream from a Jet-Engine Combustor, Including a Method of Calculating Deposition Rates on Surfaces. NACA RM E57F18, 1957.
12. Setze, Paul C.: An Analytical Study of the Equilibrium Thickness of Boric Oxide Deposits on Jet-Engine Surfaces. NACA RM E57F13b, 1957.

~~CONFIDENTIAL~~

4533

CN-6

TABLE I. - SUMMARY OF PENTABORANE PRIMARY DATA

Run	Equivalence ratio, ϕ	Fuel flow, \dot{w}_f , lb/sec	Primary air flow, \dot{w}_a , lb/sec	Atomizing air flow, lb/sec	Combustor-inlet total pressure, P_2 , lb/sq in.	Combustor-inlet velocity, V_2 , ft/sec	Combustor-air temperature, T_3 , Or	Fuel-injector pressure-loss ratio, $\frac{P_2 - P_4}{P_2}$	Combustor-exit total pressure, P_4 , lb/sq in.	Area of nozzle throat at 70° F, A_n , sq in.	Duration of data point, sec	Cooling air flow, lb/sec	Heat rejected to coolant, Q_c , Btu/sec	Combustor wall temperature, T_{of} , °F	Nozzle-wall temperature, T_{of} , °F			Internal force exerted on divider, lb	Nozzle-exit stream thrust by thrust barrel, $P_{15,bbt}$, lb	
															Station	5	8			
																				11
(a)																				
e ₁	0.316	0.134	5.51	0	48.8	60	550	0.046	46.55	12.50	84	4.77	222	575	990	880	600	350	(f)	753
2	.639	.1848	3.487	0.305	44.3	55	720	.085	40.22	12.26	36	4.05	340	810	1500	1200	800	370	66.0	665
3a	.364	.1360	4.591	.305	49.6	57	637	.090	45.15	12.30	50	3.98	218	700	1100	1000	630	440	74.8	721
3b	.577	.2080	4.446	.278	51.6	50	604	.066	48.20	12.30	526	3.98	290	920	1400	1300	820	650	79.6	767
4a	.535	.1700	3.843	.324	45.8	53	655	.081	42.08	12.30	524	4.03	271	---	1500	1300	850	570	60.2	705
4b	.482	.1544	3.868	.325	44.8	53	631	.078	41.28	12.30	518	4.09	285	---	1670	1450	910	690	59.4	689
(b)																				
(d)																				

a Supply pressure, approximately 70 lb/sq in. abs; supply temperature, approximately 70° F.

b Includes estimated heat losses to fuel-injector cooling water and nozzle-wall surfaces between entry and throat.

c Values given are maximums obtained. Steady-state values were not attained at the higher equivalence ratios tested.

d Additional force due to separation is omitted.

e Only run in which fuel injector A and uncured exhaust nozzle were used.

f Pressure data not reliable.

g Followed data point given for same run.

h Followed 46-second run at a lower equivalence ratio.

CONFIDENTIAL

TABLE II. - SUMMARY OF NOZZLE-PRESSURE-RATIO^a

DATA FOR PENTABORANE

Station	Run					
	1	3a	4b	4a	3b	2
	Equivalence ratio					
	0.318	0.364	0.482	0.535	0.577	0.639
5	0.835	0.835	0.832	0.832	0.835	0.833
6	.736	.738	.733	.732	.735	.734
7	.613	.616	.587	.575	.616	.616
8	.511	.514	.492	.481	.483	.519
9	.450	.454	.434	.425 ^b	.441	.456
10	.361	.338	.344	.337	.336	.369
11	----	.275	.258	.252	.258	.273
12	----	.195	.176	.173	.183	.200
13	----	.102	.099	.096	.096	.112
14	----	^c .104	^c .108	^c .104	^c .096	^c .117
Base	----	.123	.125	.122	.126	.154
Plenum	----	.113	.119	.115	.113	.144

^aPressure ratio is nozzle static pressure divided by combustor-exit stagnation pressure.

^bVaried between 0.425 and 0.457.

^cPossible flow separation.

CONFIDENTIAL

TABLE III. - SUMMARY OF PENTABORANE PERFORMANCE DATA

Run	Equip- alence ratio	Static temper- ature at nozzle throat, t_8 , OR	Corrected tempera- ture at nozzle throat, t_8 , corr., OR	Ratio of specific heats, γ_8	Fluid specific con- stant, R_8	Combus- tion effi- ciency, η_c , percent	Boric oxide condensed at nozzle throat, percent	Air specific impulse		Nozzle- exit stream thrust com- puted from pressure data, F_{15} , lb	Ratio of nozzle- exit stream thrust, $\frac{F_{15, bbl}}{F_{15}}$	Air specific stream thrust at nozzle exit (a)		Diver- gence effi- ciency, η_w	Diver- gence effi- ciency ratio
								S_a , sec	S_a , corr., sec			F_{15}/w_a , sec	$\left(\frac{F_{15}}{w_a}\right)_{corr}$, sec		
1	0.318	2470	2450	1.272	51.5	101.1	d100	129.2	128.8	780	0.965	141.4	142.3	d80	d1.00
3a	.364	2820	2750	1.263	51.2	102.6	d100	138.5	137.1	745	.968	152.5	152.2	80	1.01
4b	.482	3100	3103	1.254	51.3	d100	58	146.8	146.8	672	1.025	160.6	161.0	69	.87
4a	.535	3260	3240	1.248	51.3	d100	d42	151.0	150.6	686	1.027	164.7	164.9	69	.87
3b	.577	3230	3238	1.250	52.3	100.8	d0	152.0	152.2	785	.977	166.2	166.9	69	.87
3b	.577	3260	3268	1.250	52.3	d100	4	152.0	152.2	785	.977	166.2	166.9	69	.87
2	.659	3460	3467	1.245	52.2	99.9	d0	158.0	158.2	661	1.006	174.2	175.6	79	1.00

aStream thrust computed from pressure data.

b $\eta_w = \frac{(\text{SpA for pentaborane})}{(\text{SpA for one-dimensional isentropic flow of a perfect gas at constant } \gamma)}$ 100c η_w pentaborane

dAssumed.

CONFIDENTIAL

TABLE IV. - EFFECT OF ABRUPT CONDENSATION STEP ON
PROPERTIES OF COMBUSTION PRODUCTS^a

Run	3b	4a
Equivalence ratio, ϕ	0.577	0.535
Pressure ratio, p'/P	0.58	0.64
Static pressure ratio, $(\Delta p)'/p'$	-0.068	-0.071
Mach number at wall, M'	0.95	0.90
Fraction of boron oxide condensed, $\frac{(\Delta w_l)'}{w_{B_2O_3}}$	0.04	0.10
Fluid constant ratio, $(\Delta R)'/R'$	-0.002	-0.005
Static temperature ratio, $(\Delta t)'/t'$	$\ll (\Delta p)'/p'$	$\ll (\Delta p)'/p'$
Velocity ratio and Mach number ratio, $(\Delta V)'/V'$ and $(\Delta M)'/M'$	$\approx -(\Delta p)'/p'$	$\approx -(\Delta p)'/p'$
Total pressure, $(\Delta P)'/P'$	-0.005	-0.008

^aSymbols used in table:

Prime represents mean value of a property at location of phase change.

$(\Delta)'$ represents change in value of a property resulting from phase change.

CONFIDENTIAL

• Thermocouple

⚡ Water sprays

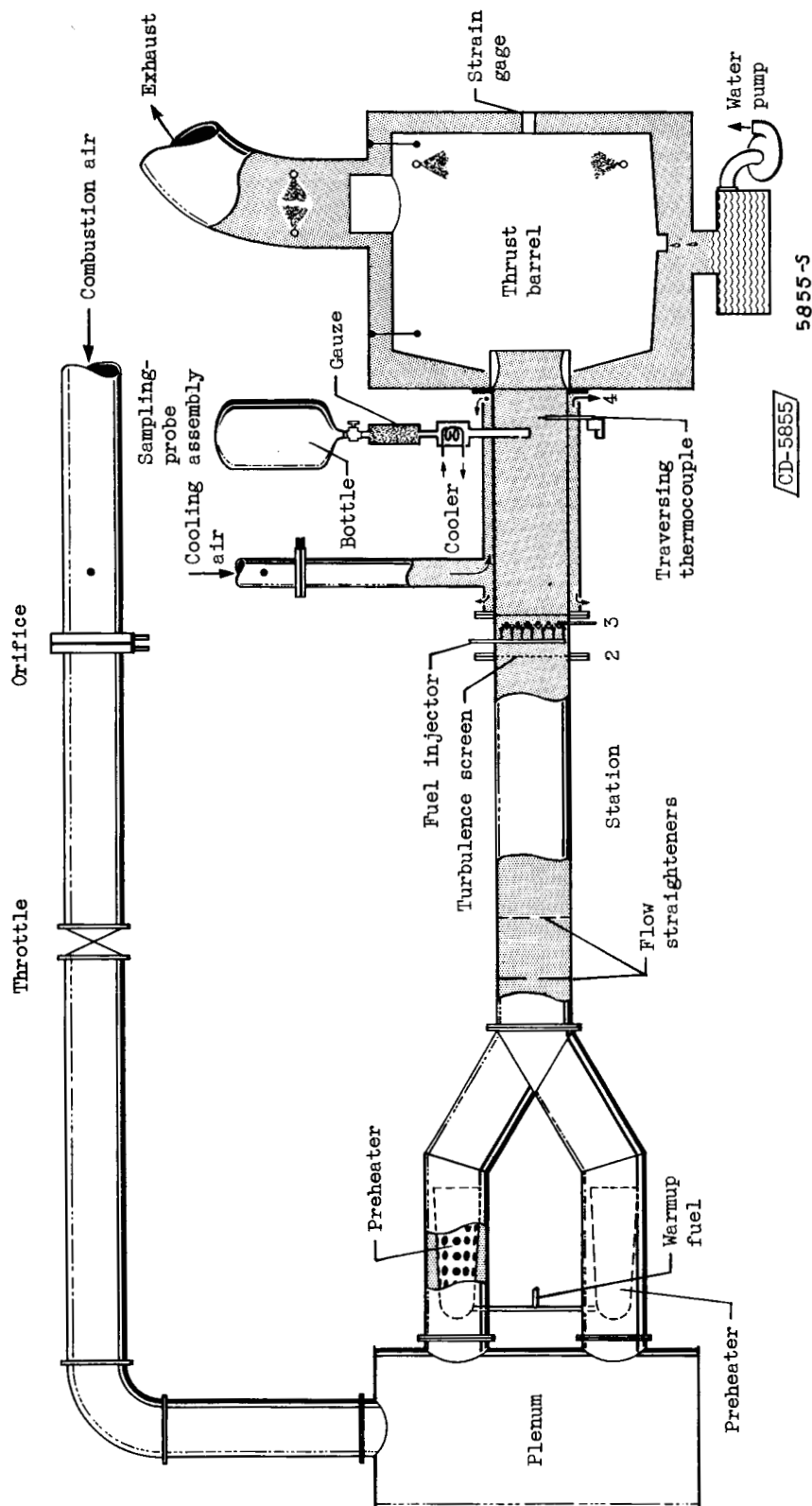
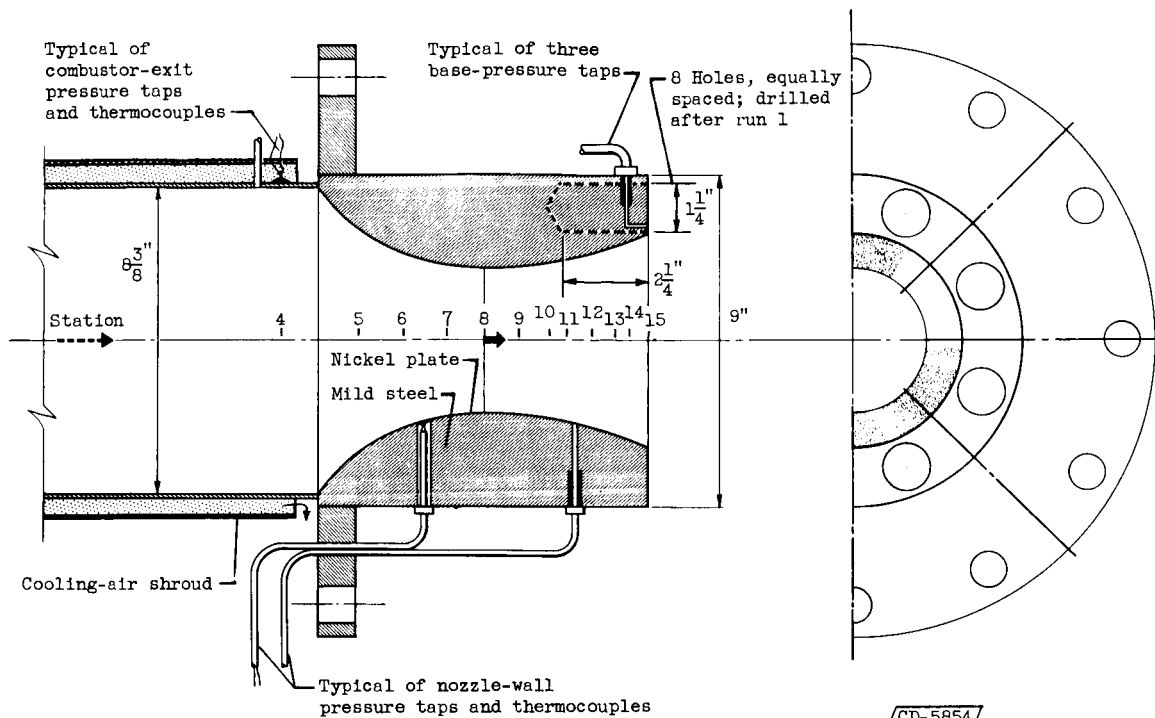


Figure 1. - Apparatus assembly.



Station	Distance from throat, in.	Area Throat area	Static-pressure taps	Thermocouples
4	6.00	4.4	4	4
Inlet	4.00	4.4	0	0
5	2.20	1.300	1	4
6	1.41	1.097	2	0
7	.70	1.012	2	0
8	0	1.000	4	4
9	.48	1.012	2	0
10	1.00	1.050	2	0
11	1.52	1.131	4	4
12	2.12	1.269	2	0
13	2.79	1.519	2	0
14	3.01	1.630	4	4
15	3.10	1.680	0	0

Figure 2. - Diagram and dimensions of nozzle.

DECLASSIFIED

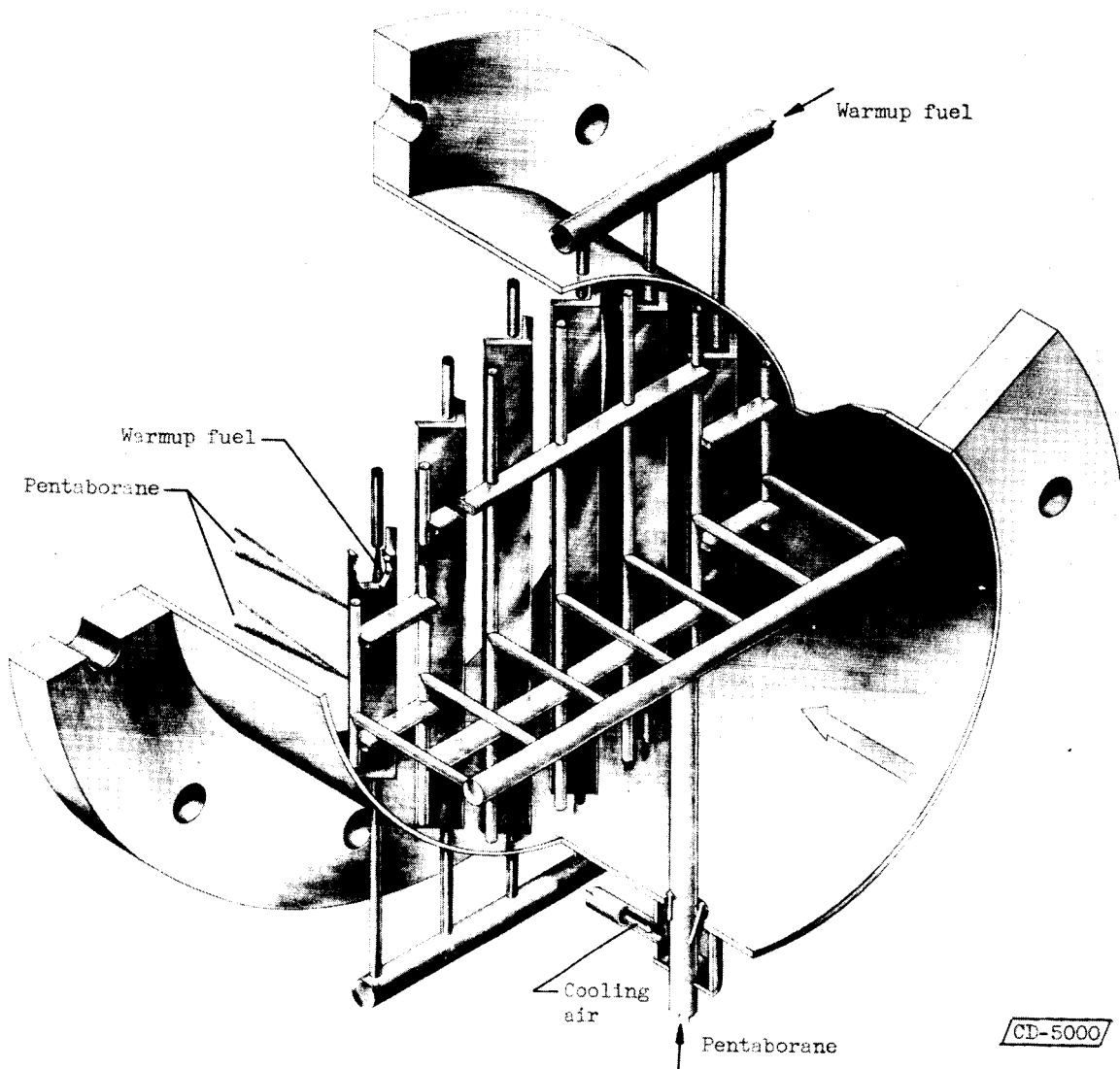


Figure 3. - Fuel injector A.

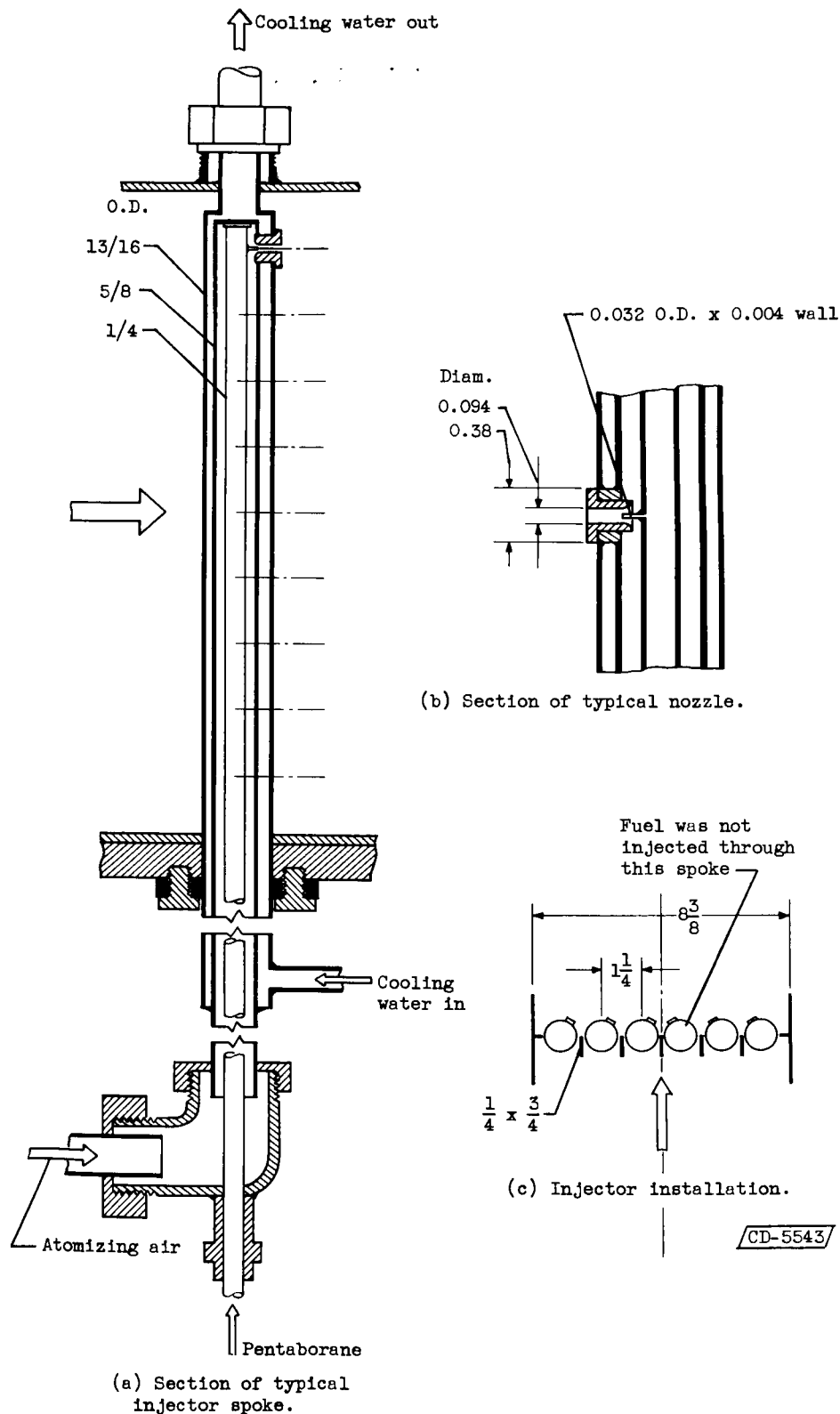


Figure 4. - Fuel injector B. (All dimensions in inches.)

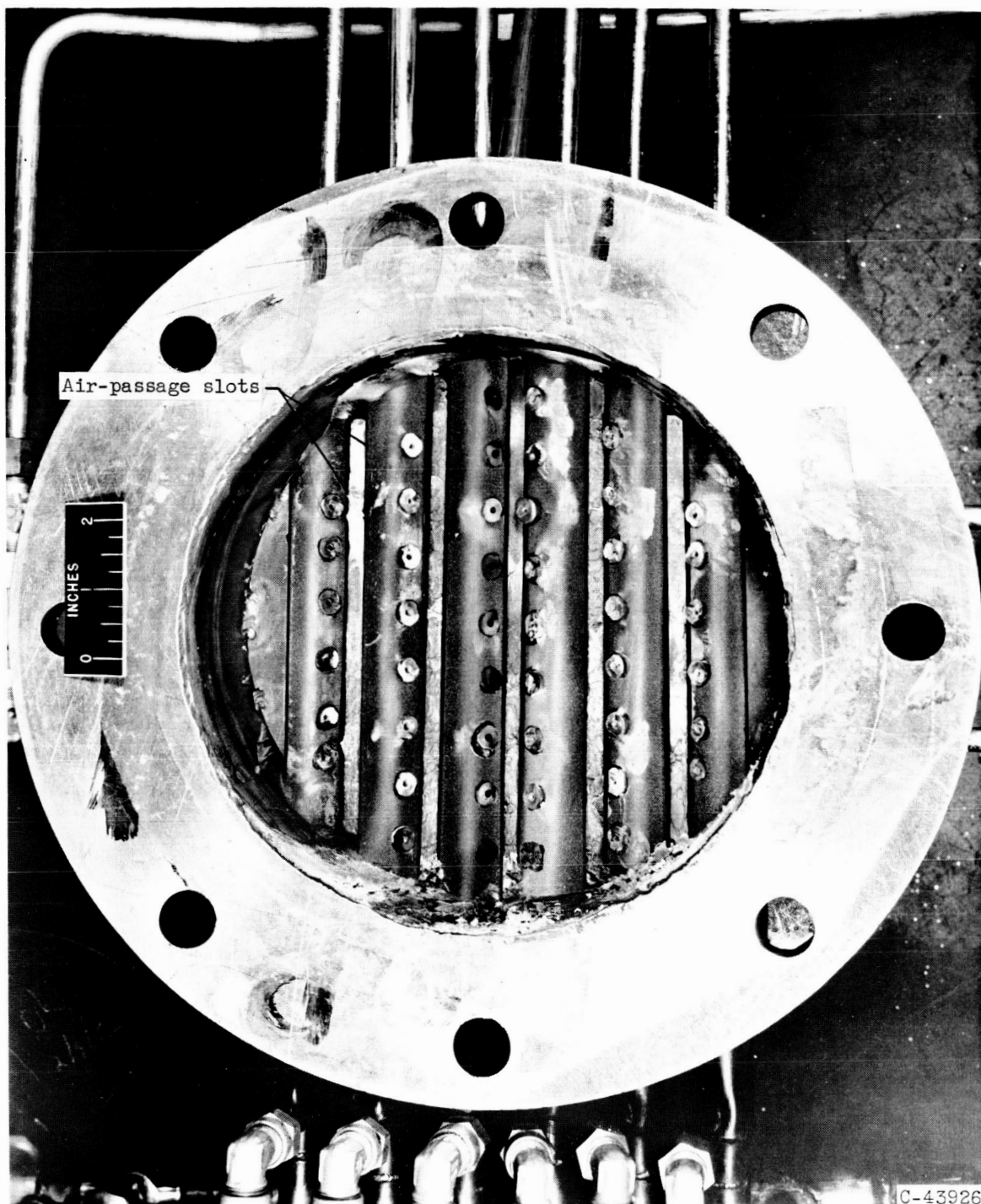


Figure 5. - Fuel injector B after a pentaborane fuel test.

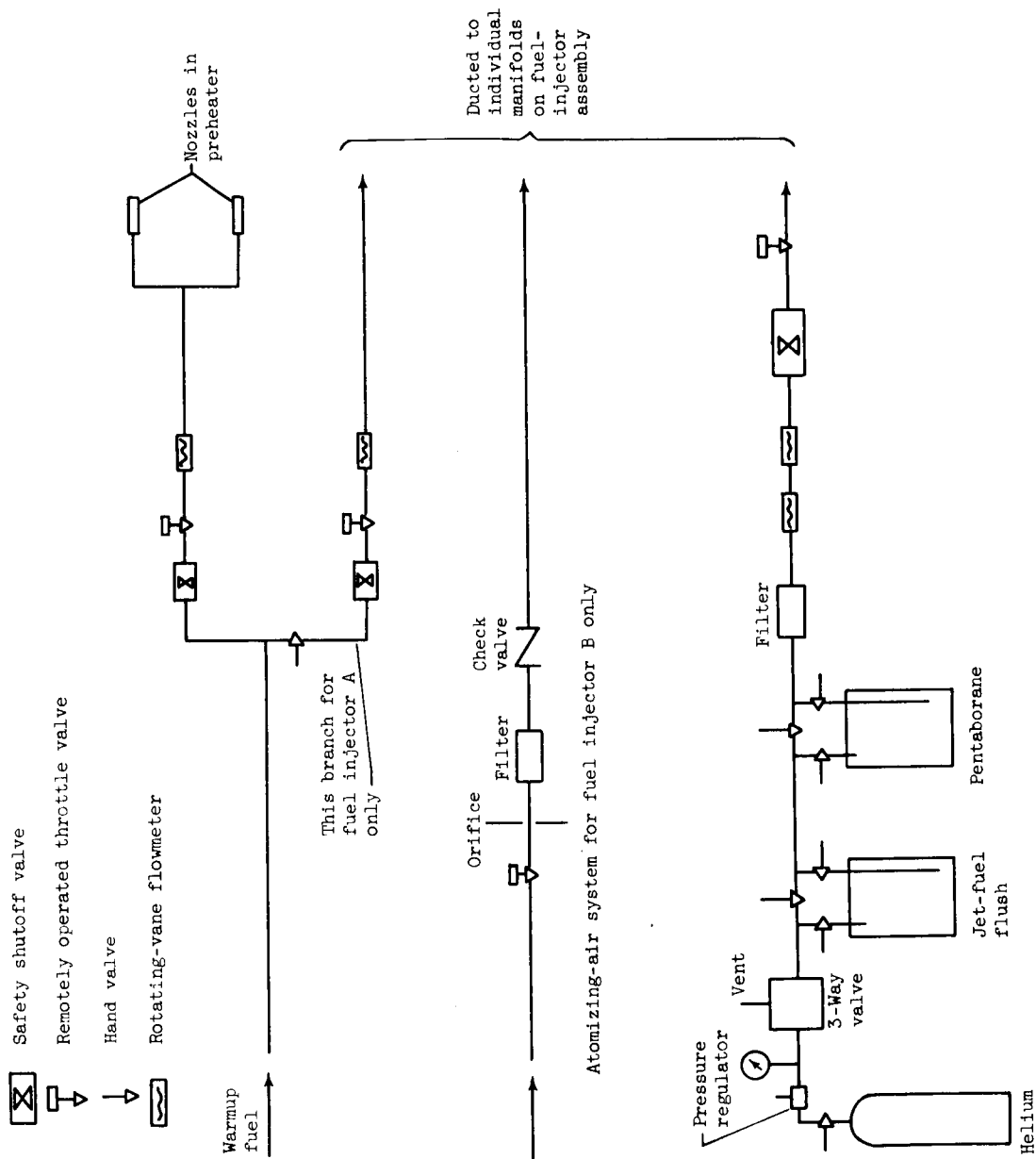
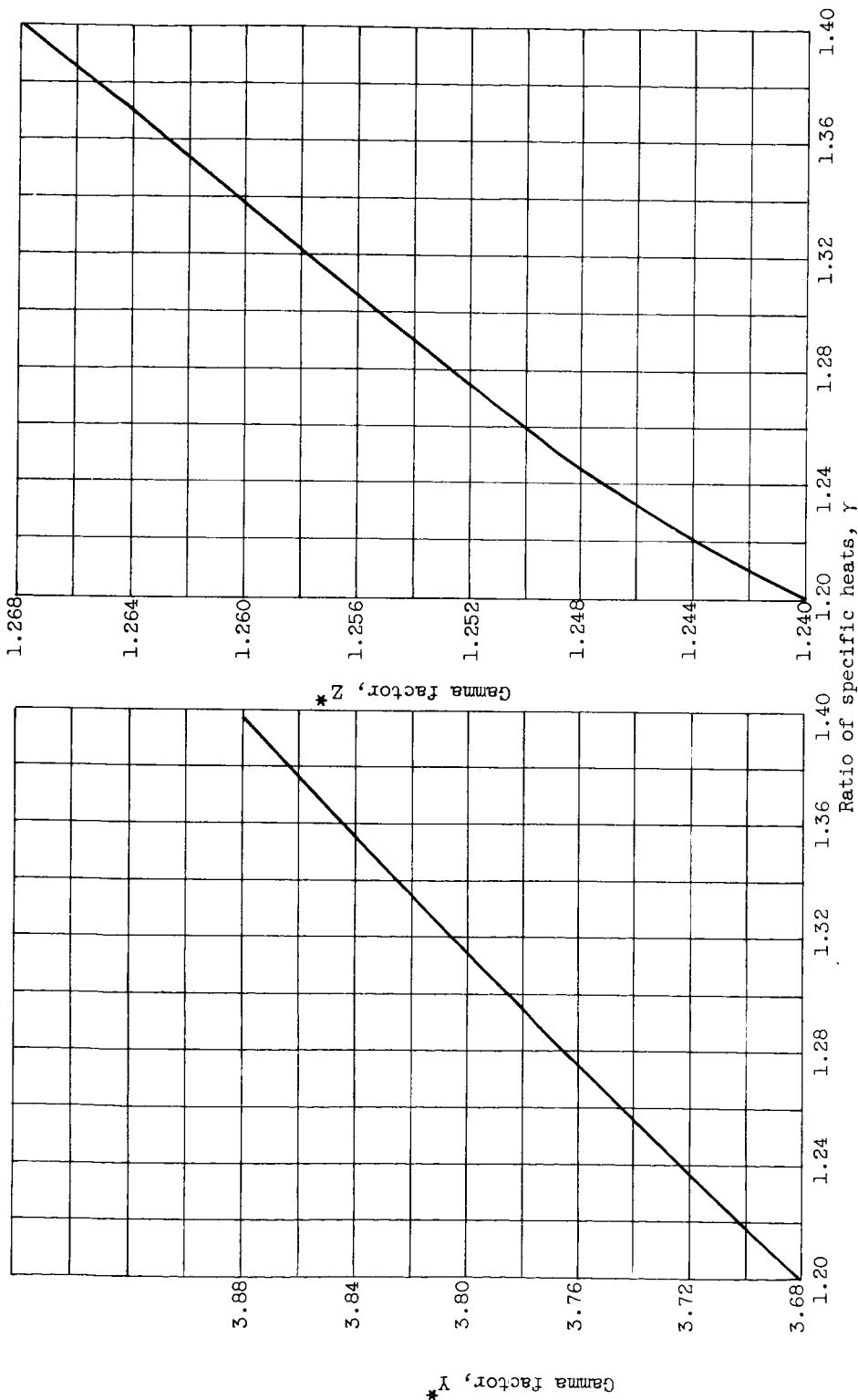


Figure 6. - Fuel system.

CONFIDENTIAL

4533

CN-7 back



(a) Continuity equation. Gamma factor

$$Y^* = \sqrt{\frac{\gamma g}{\left(\frac{\gamma + 1}{2}\right)^{\frac{\gamma + 1}{\gamma - 1}}}}$$

(b) Momentum equation. Gamma factor

$$Z^* = 2^{\frac{\gamma}{\gamma - 1}} (\gamma + 1)^{\frac{1}{1 - \gamma}}$$

Figure 7. - Gamma factors for continuity and momentum equations.

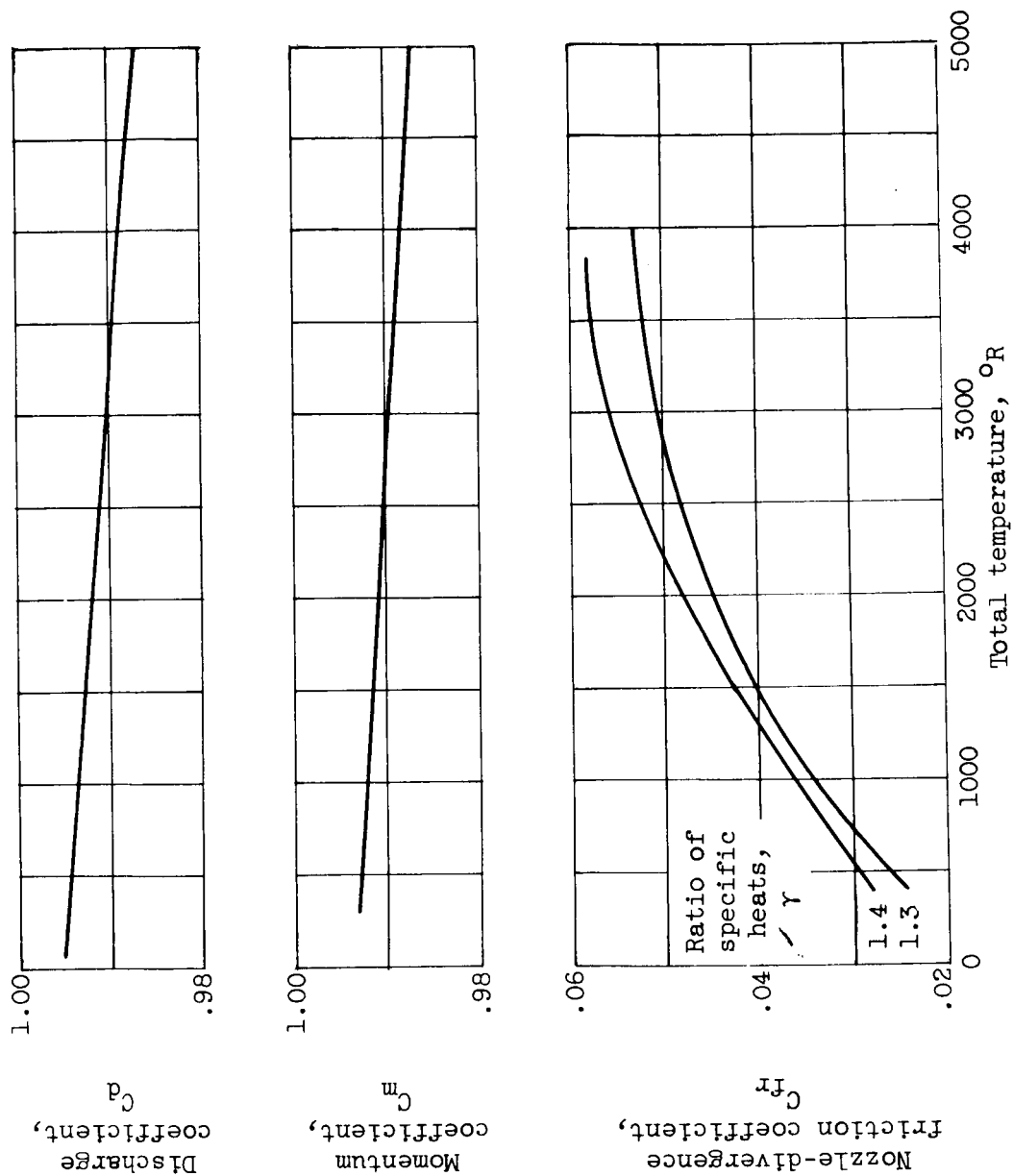


Figure 8. - Coefficients that express deviation from one-dimensional ideal flow existing in nozzle.

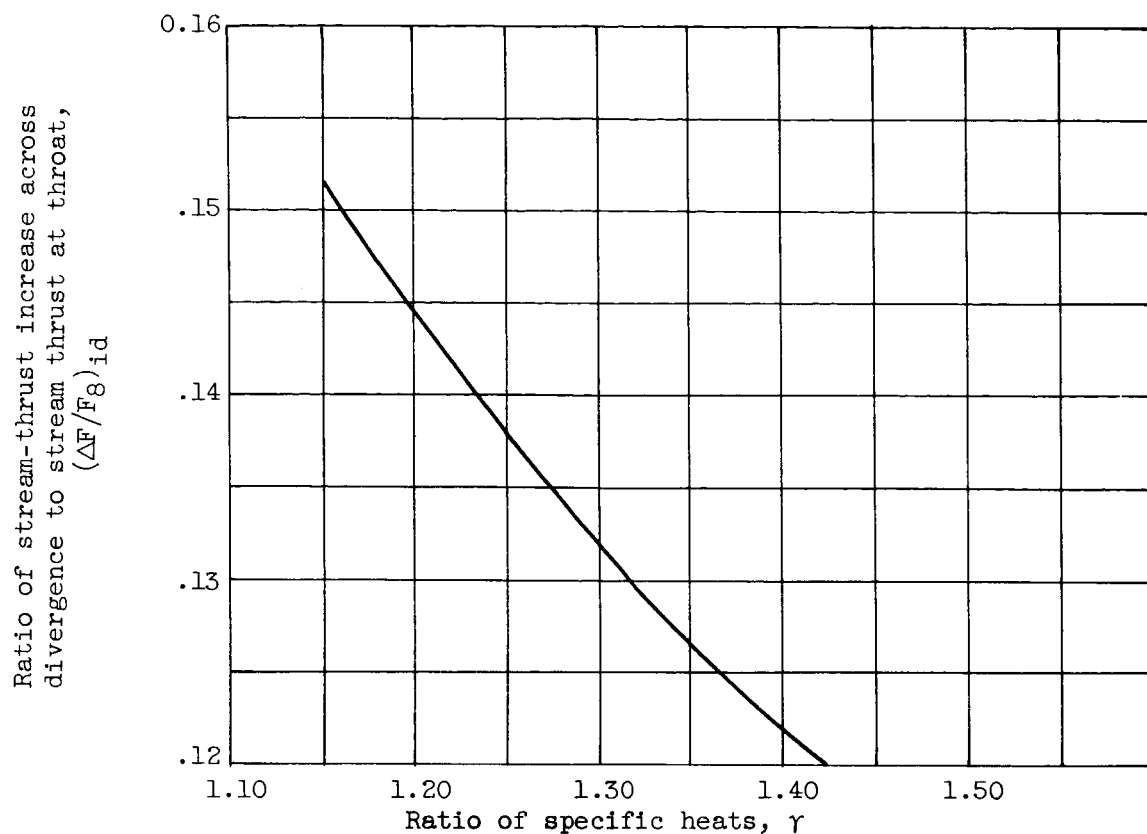


Figure 9. - Effect of specific-heats ratio on divergence stream thrust for ideal one-dimensional flow. Nozzle-exit-to-throat area ratio, 1.68.

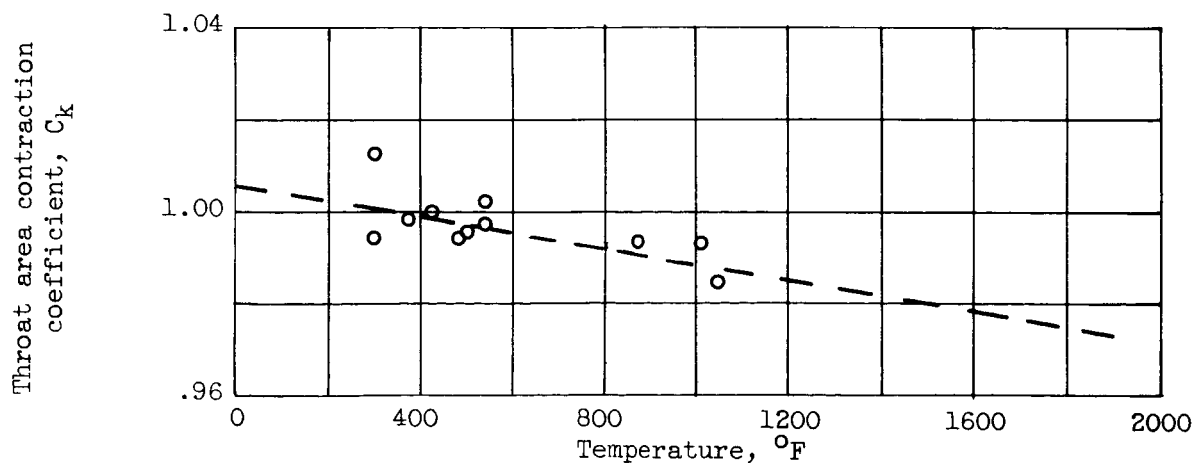


Figure 10. - Effect of wall temperature at nozzle throat on throat area for warmup-fuel products of combustion.

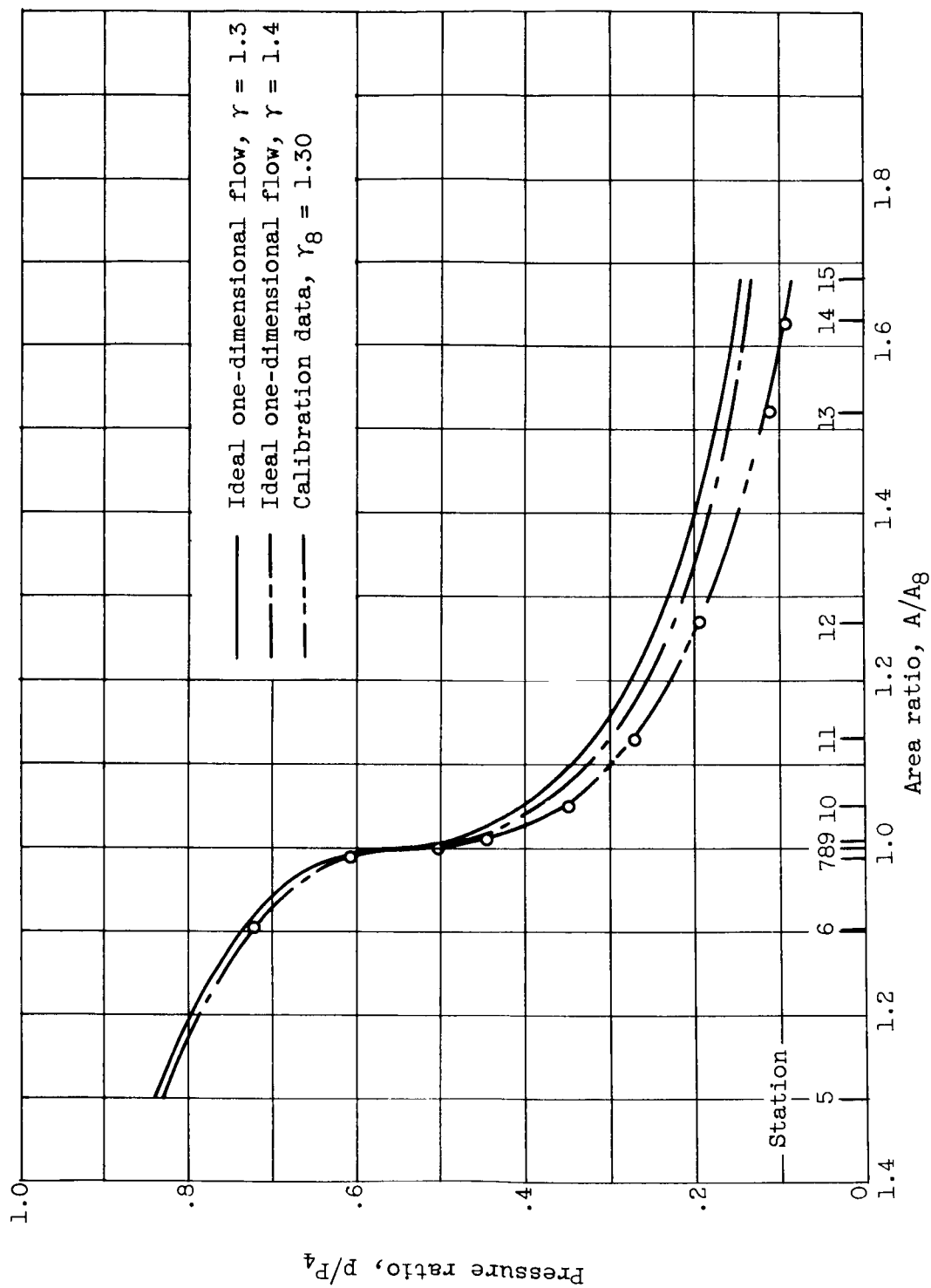


Figure 11. - Comparison of one-dimensional and measured three-dimensional flow in nozzle.

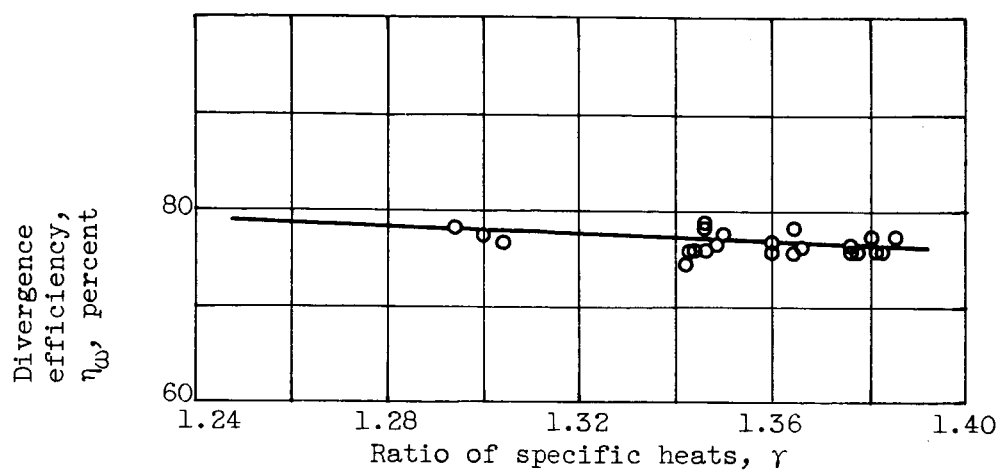
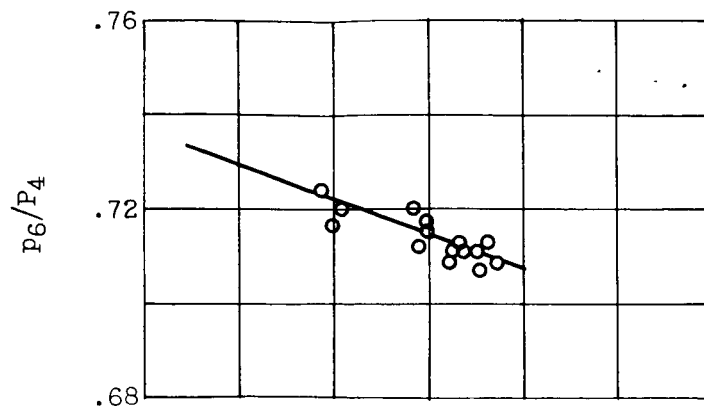
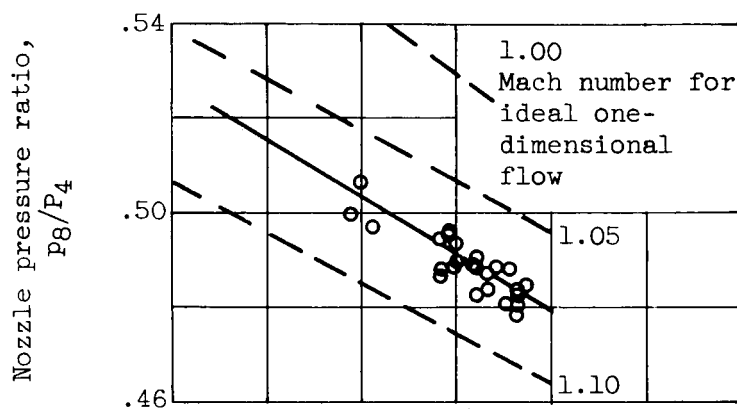
~~CONFIDENTIAL~~

Figure 12. - Comparison of actual to ideal stream thrust produced in divergent portion of exhaust nozzle for warmup-fuel products of combustion.

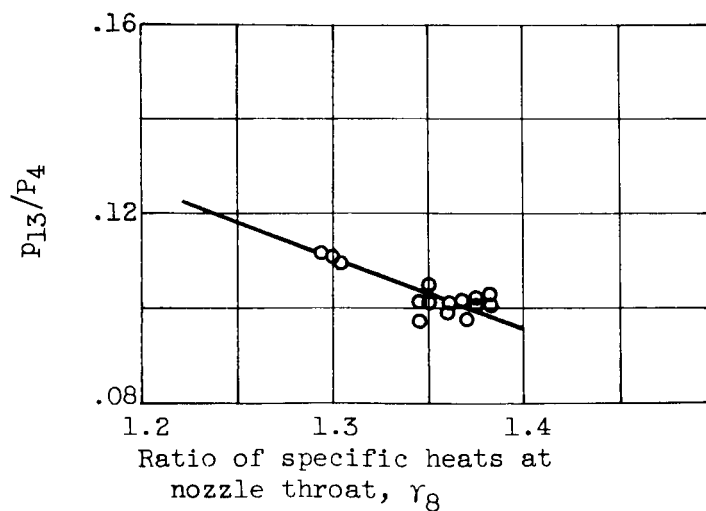
CONFIDENTIAL



(a) Station 6.



(b) Station 8 (throat).



(c) Station 13.

Figure 13. - Nozzle-wall static-pressure data for warmup-fuel products of combustion.

CONFIDENTIAL

DECLASSIFIED

DECLASSIFIED

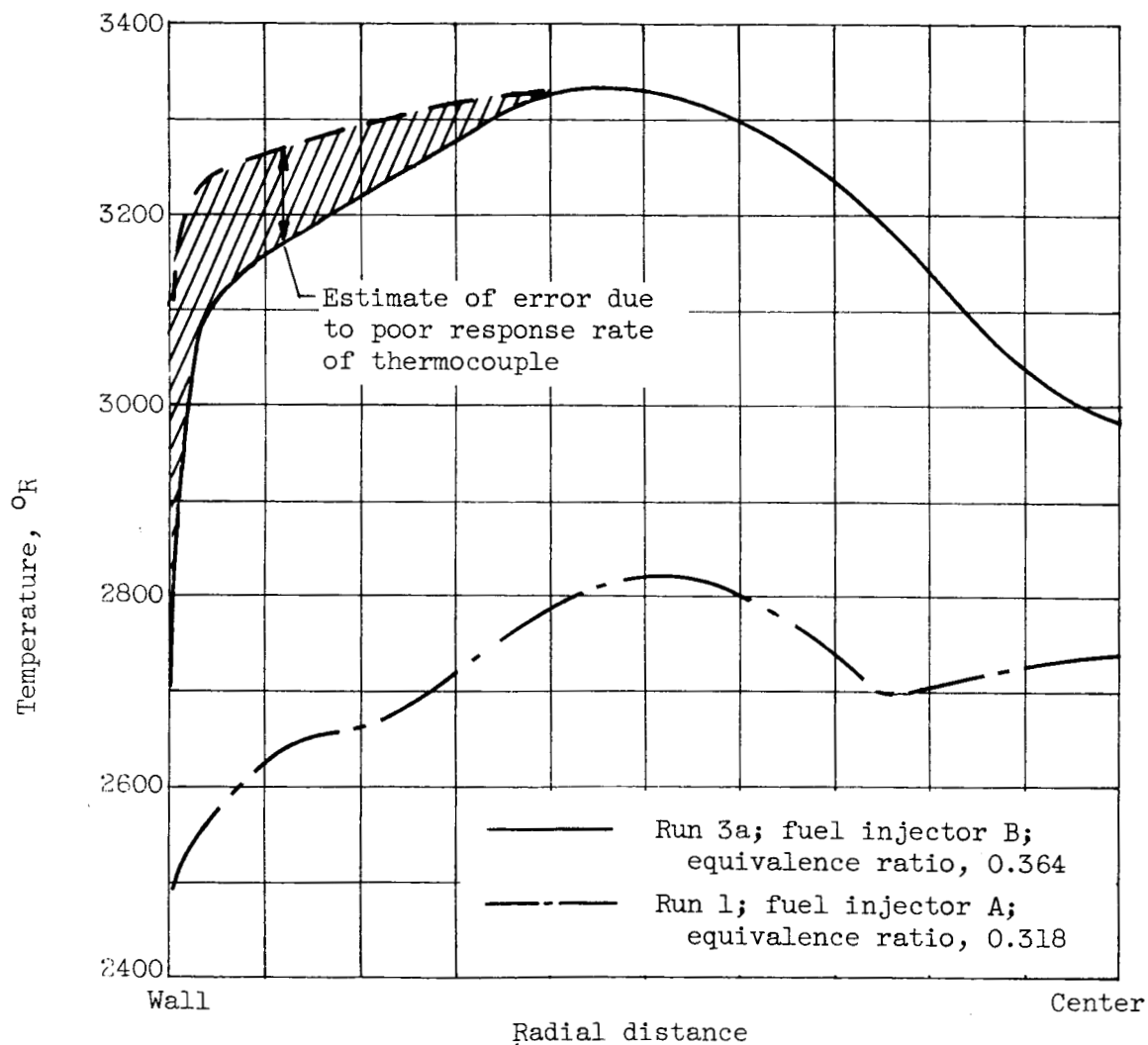
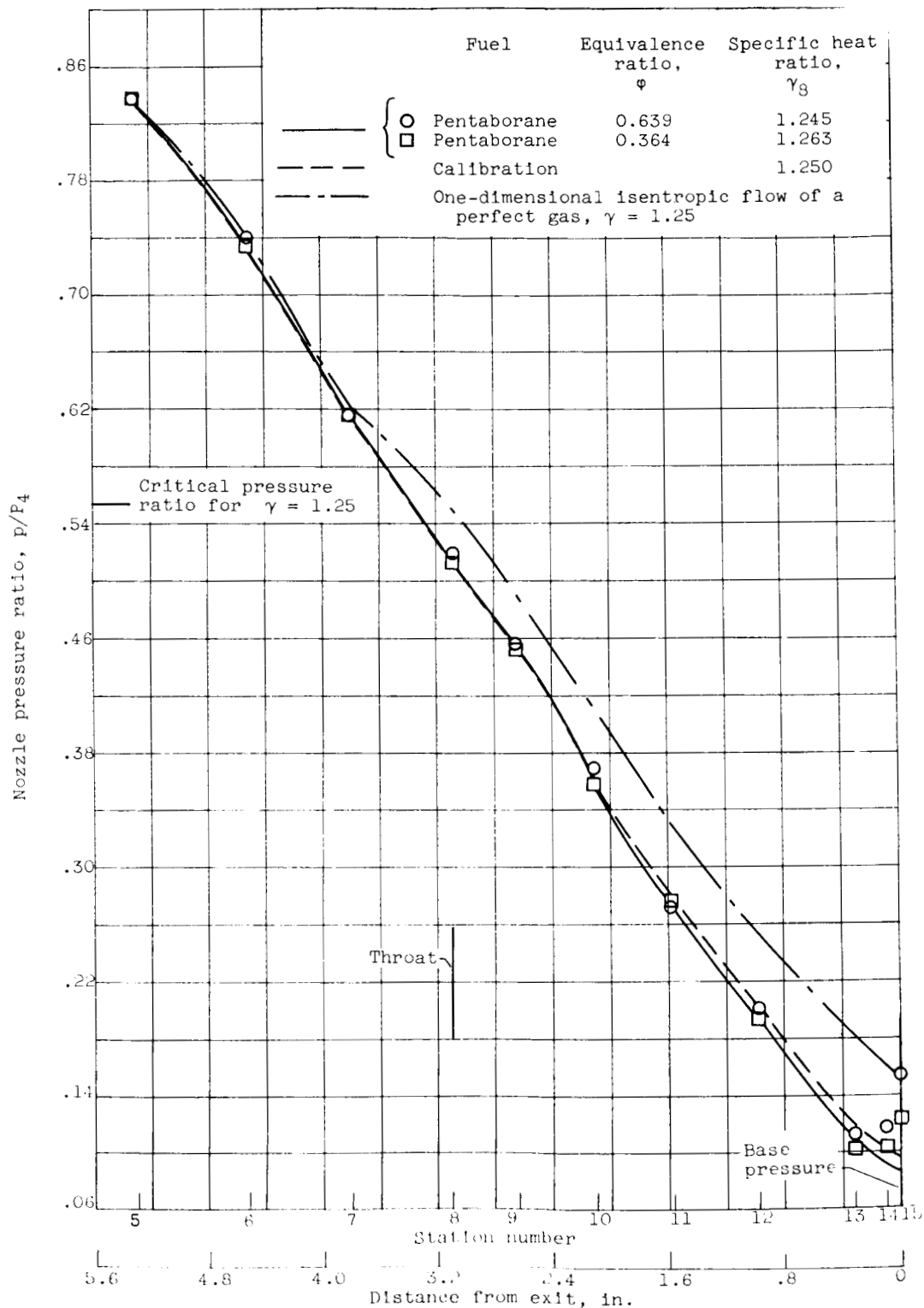
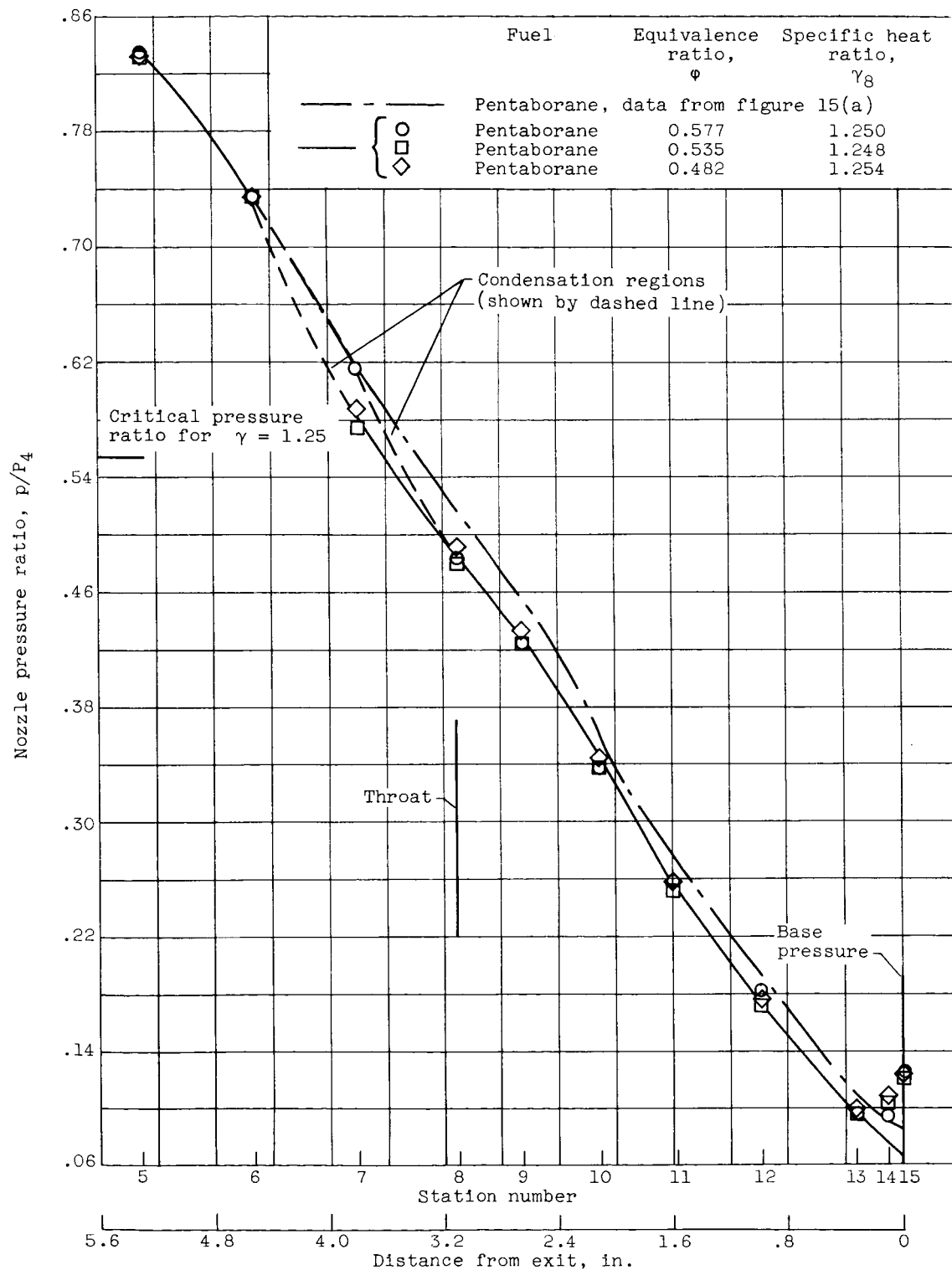


Figure 14. - Combustor-exit temperature profile obtained with exposed-bead thermocouple uncorrected for heat losses. Fuel, pentaborane.



(a) Without condensation.

Figure 15. - Nozzle-wall static-pressure data.



(b) With condensation.

Figure 15. - Concluded. Nozzle-wall static-pressure data.

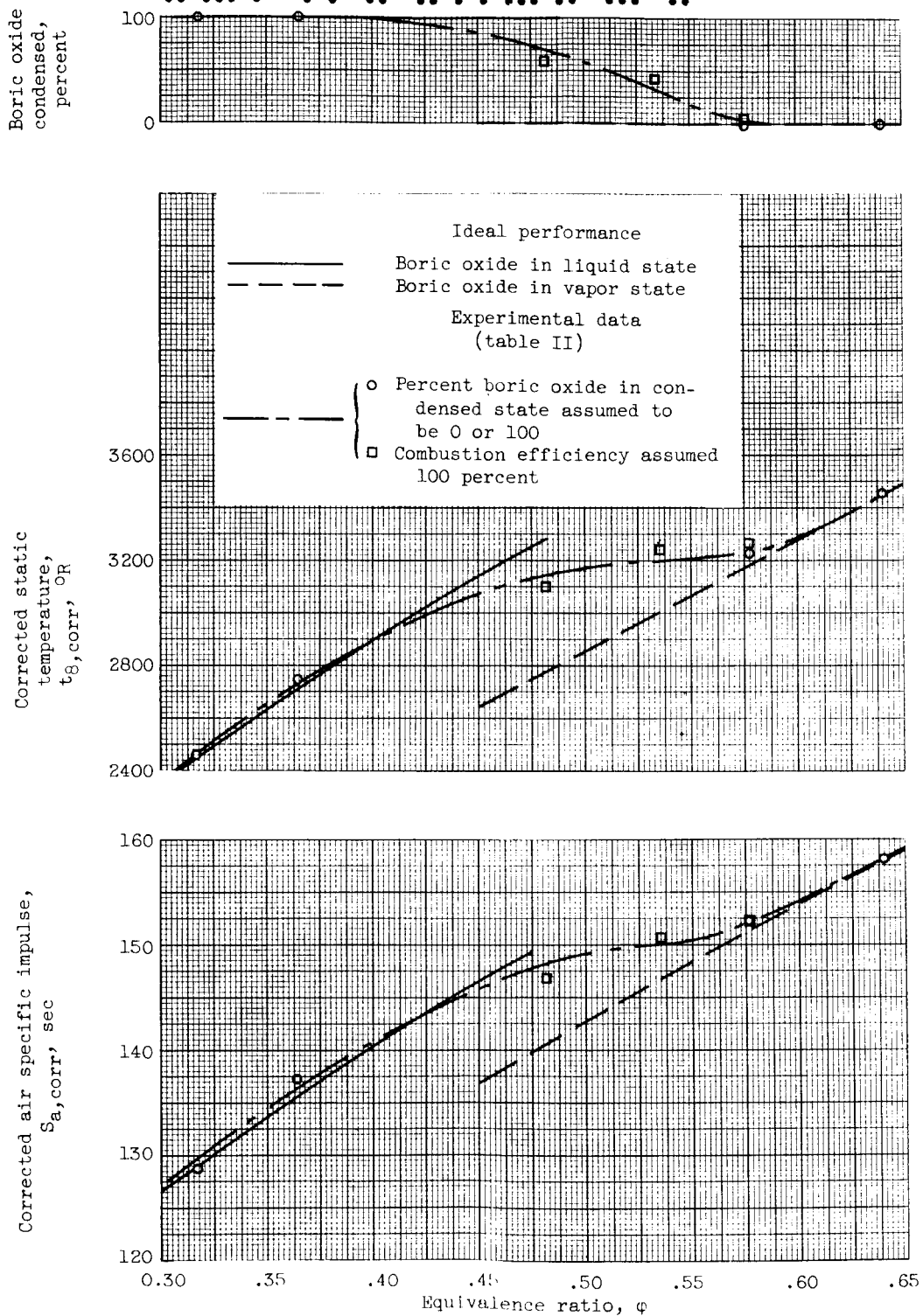


Figure 16. Comparison of ideal and experimental performance of penta-borane at nozzle throat. Experimental data corrected for heat lost through combustor walls. Corrected combustor-inlet air temperature, 360° R; combustor pressure, approximately 3 atmospheres.

CONFIDENTIAL

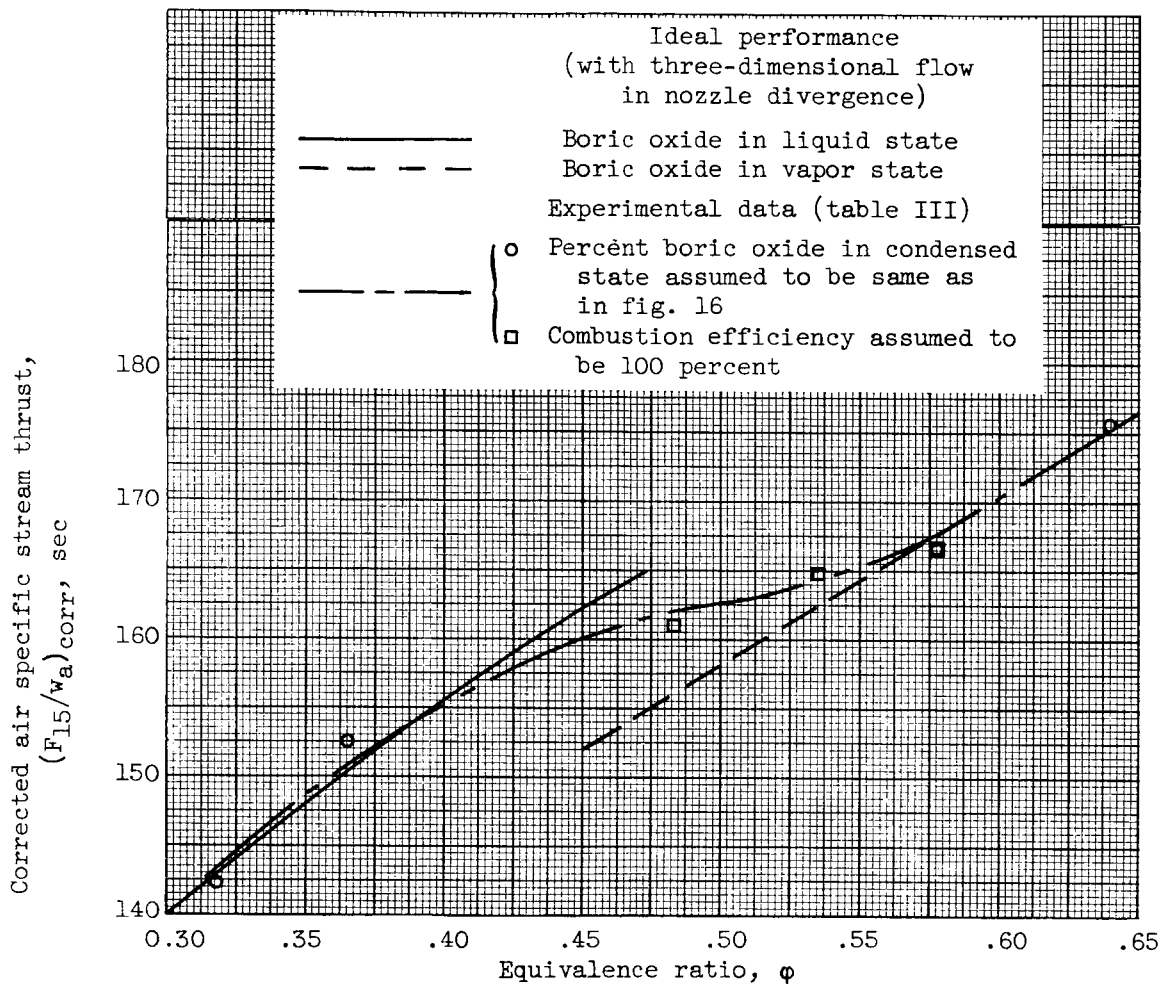


Figure 17. - Comparison of ideal and experimental air specific thrusts of pentaborane at nozzle exit. Experimental data corrected for heat lost through combustor walls. Corrected inlet-air temperature, 360° R; combustor pressure approximately 3 atmospheres. Friction losses omitted.

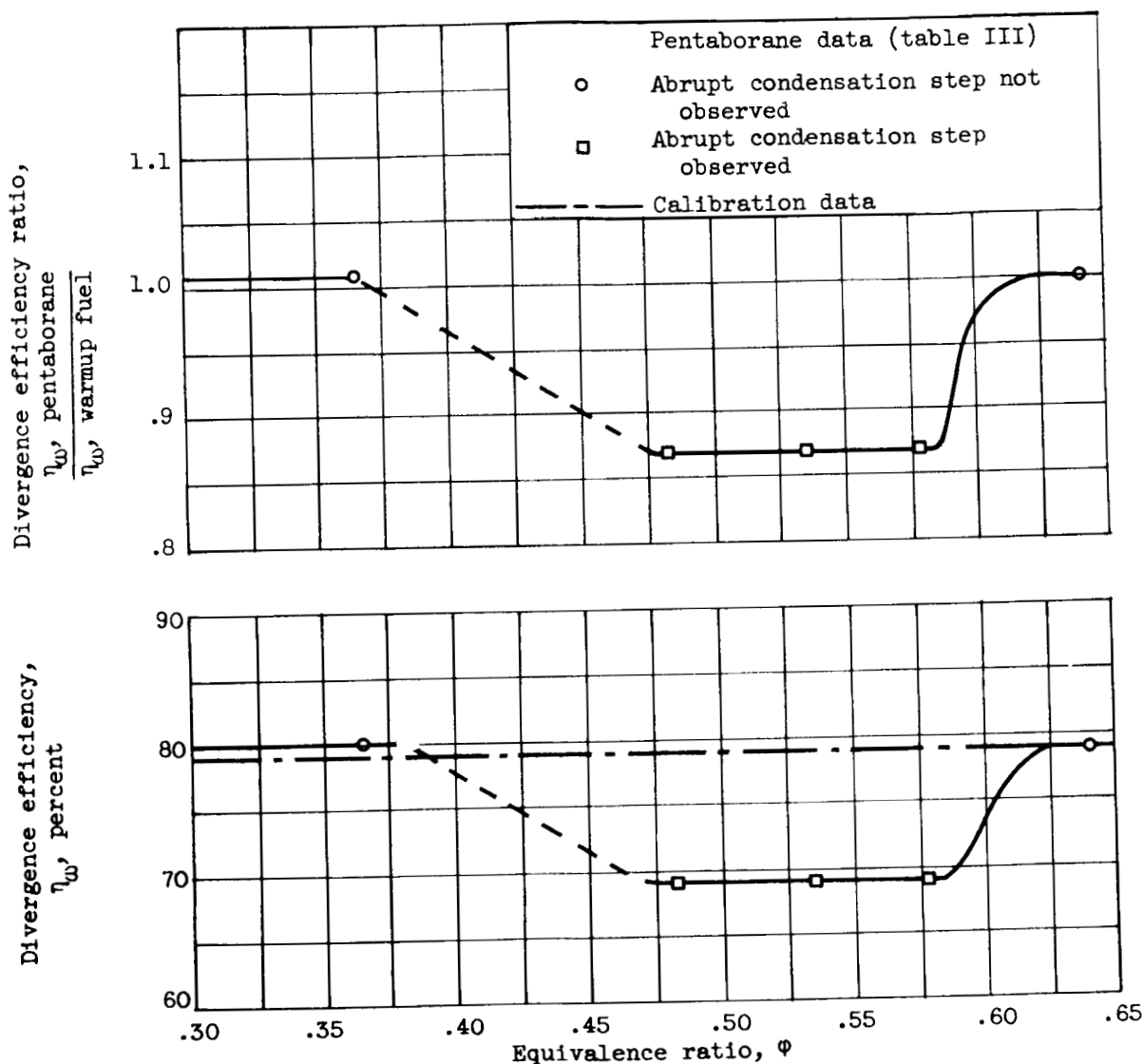


Figure 18. - Thrust producing effectiveness of nozzle divergence.
Frictional losses omitted.

DECLASSIFIED

DECLASSIFIED

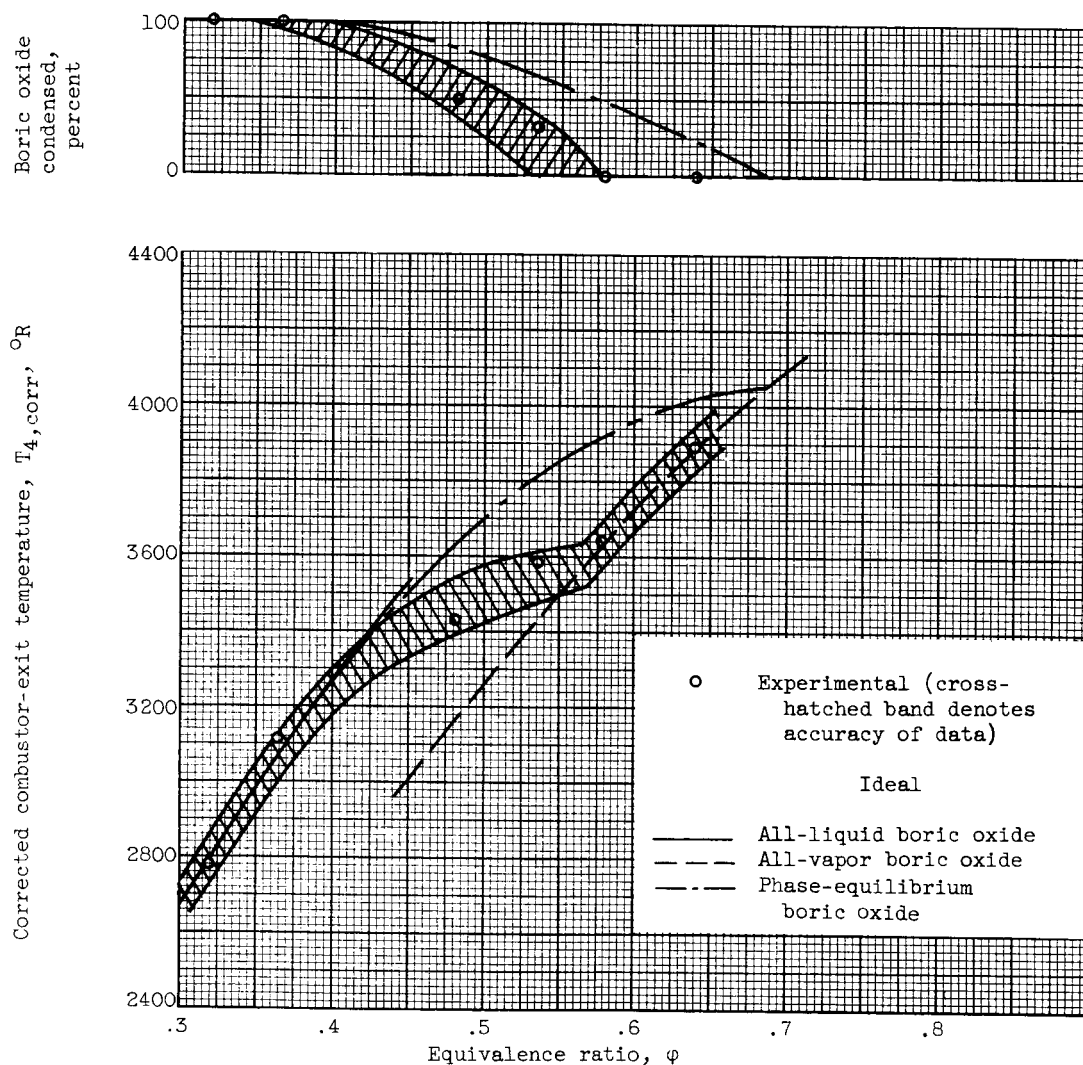


Figure 19. - Comparison of ideal and experimental performance data at combustor exit. Fuel, pentaborane; combustor-inlet temperature, 360° R; combustor pressure, 3 atmospheres.

DECLASSIFIED

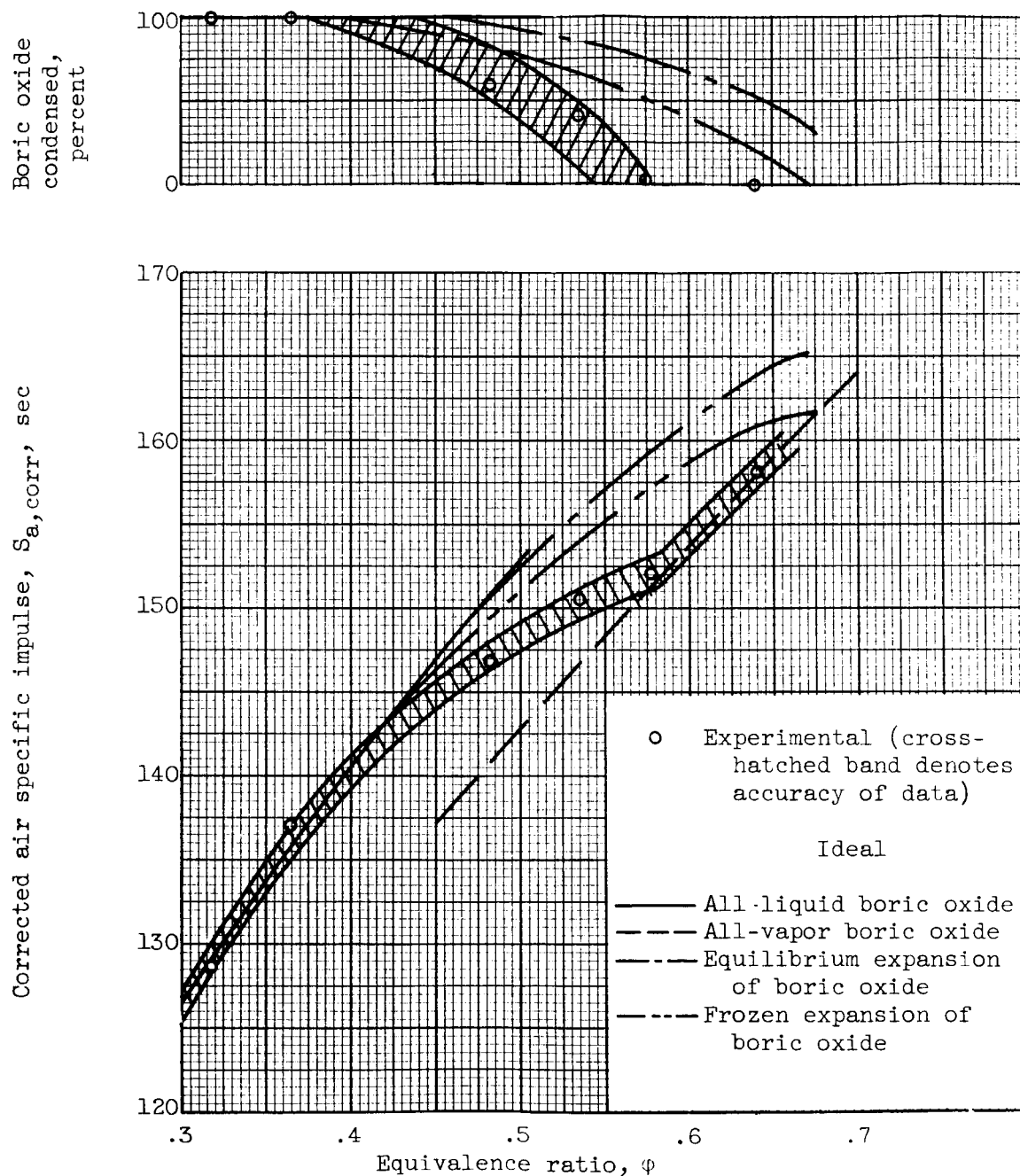


Figure 20. - Comparison of ideal and experimental data at nozzle throat. Fuel, pentaborane; combustor-inlet air temperature, 360°R ; combustor pressure, 3 atmospheres.

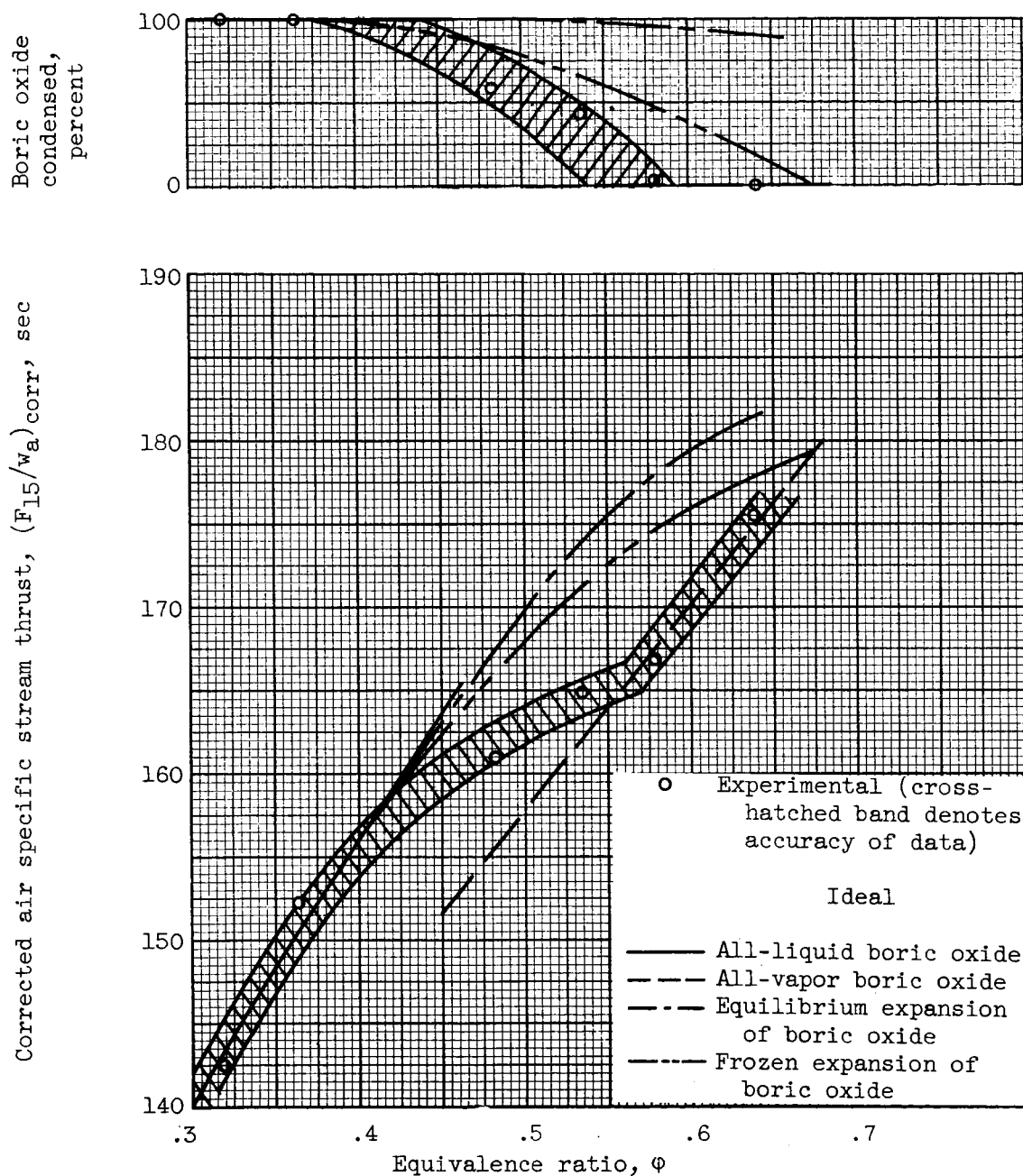


Figure 21. - Comparison of ideal and experimental performance data at nozzle exit. Fuel, pentaborane; combustor-inlet air temperature, 360°R ; combustor pressure, 3 atmospheres.

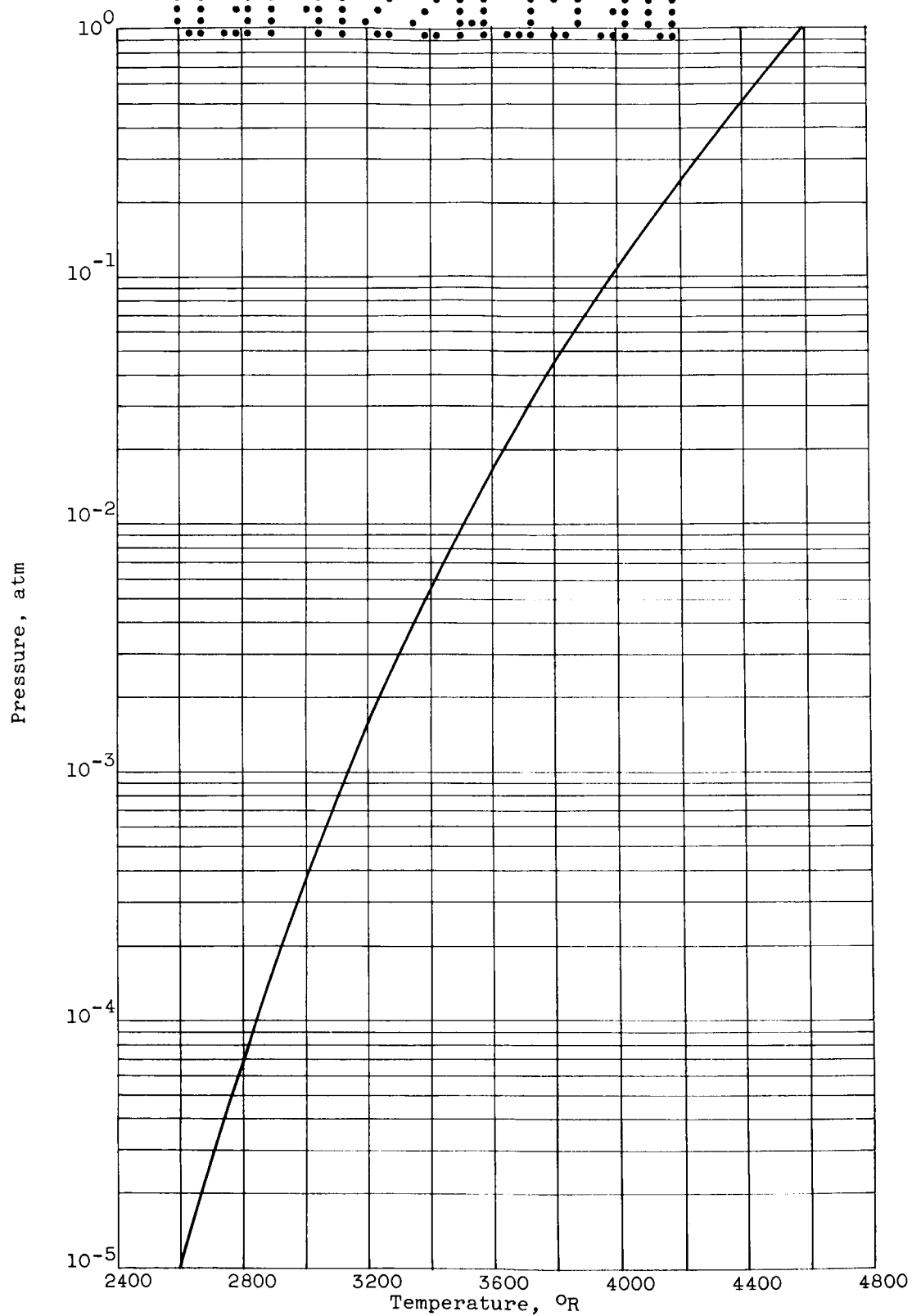


Figure 22. - Vapor-pressure data for boric oxide from reference 2.

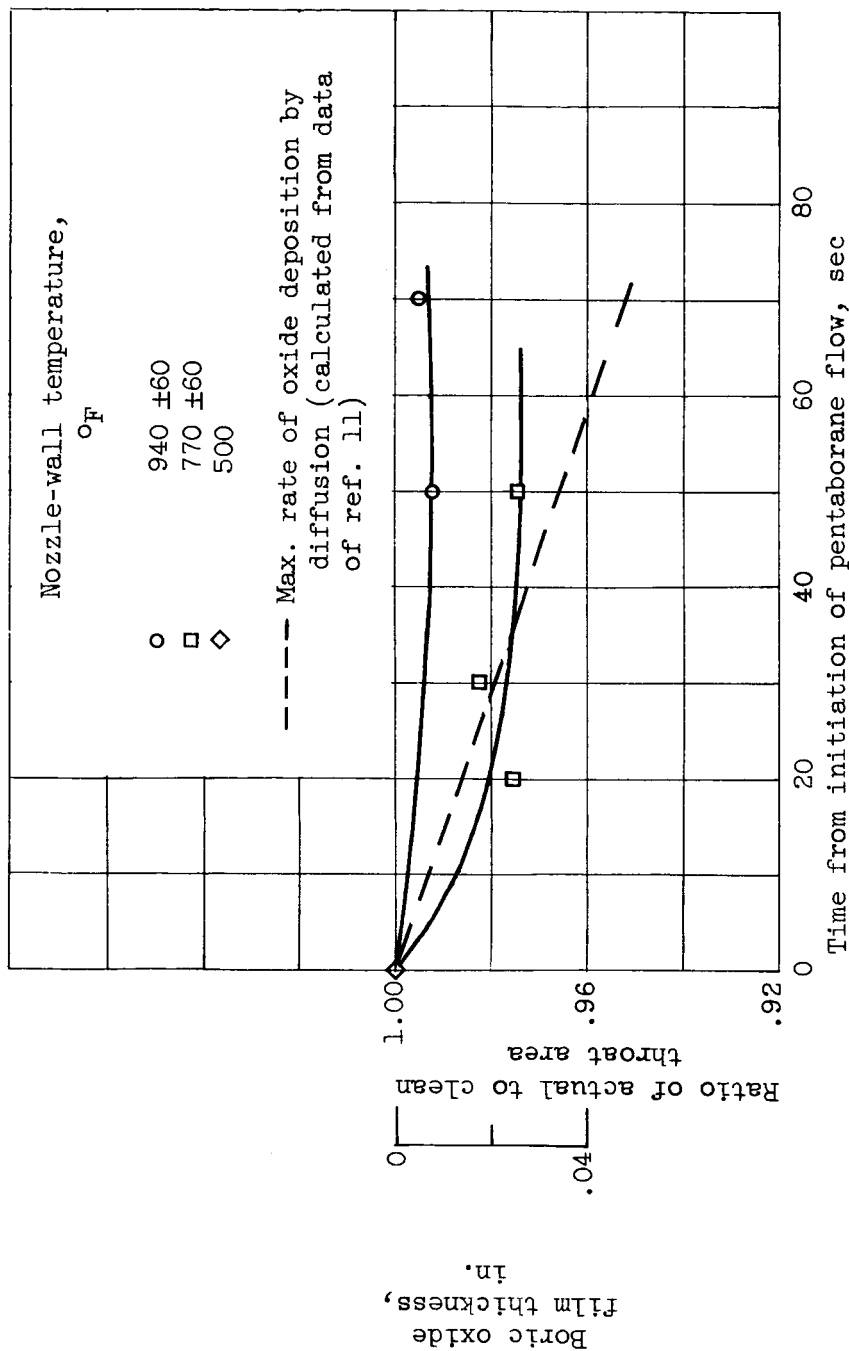


Figure 23. - Correlation of nozzle-throat surface temperature with boric oxide film thickness at throat. Nozzle-throat static temperature, 2400° to 2800° R; static pressure, 1.7 atmospheres.

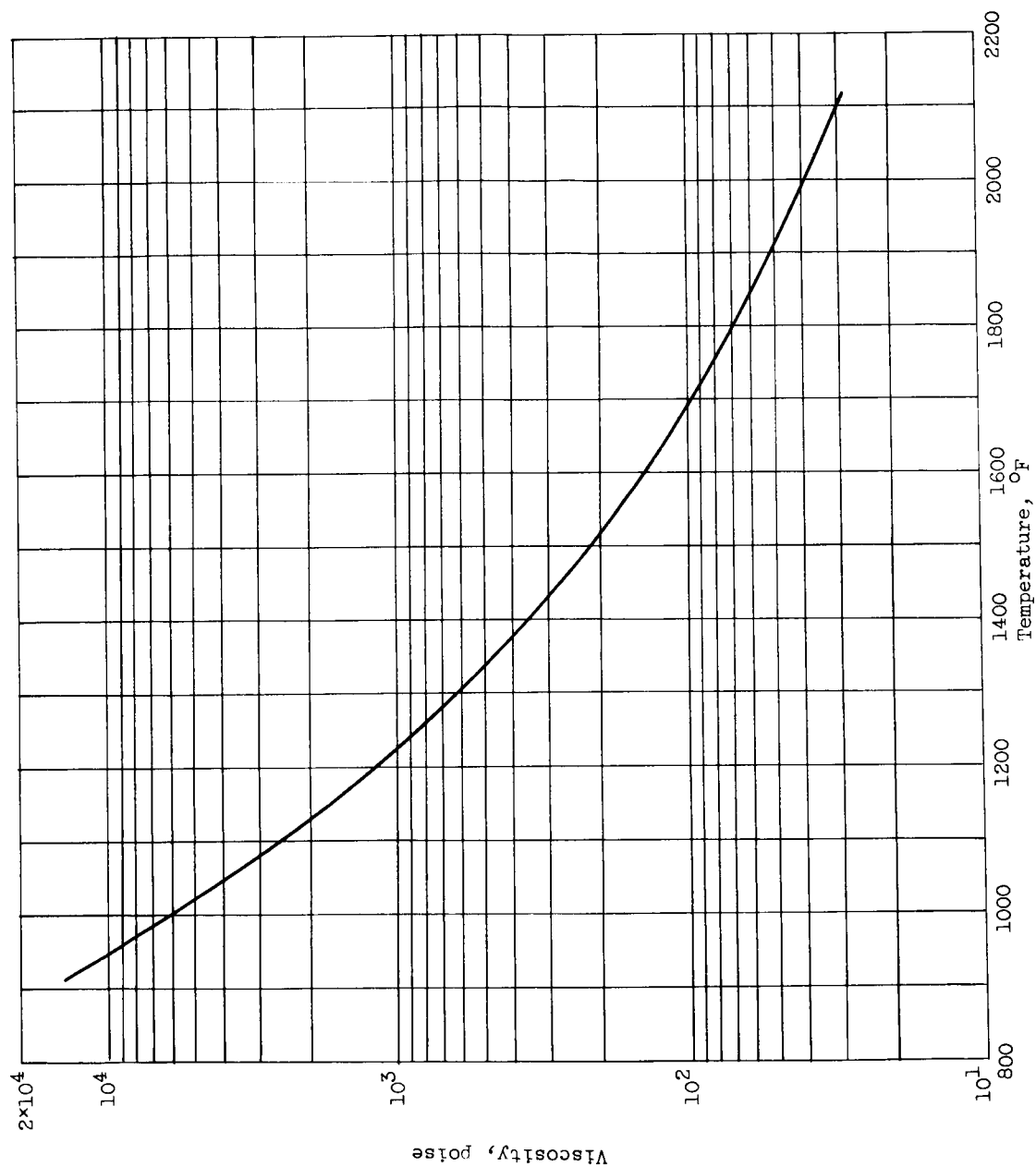


Figure 24. - Viscosity of boric oxide. (Data obtained from ref. 2.)

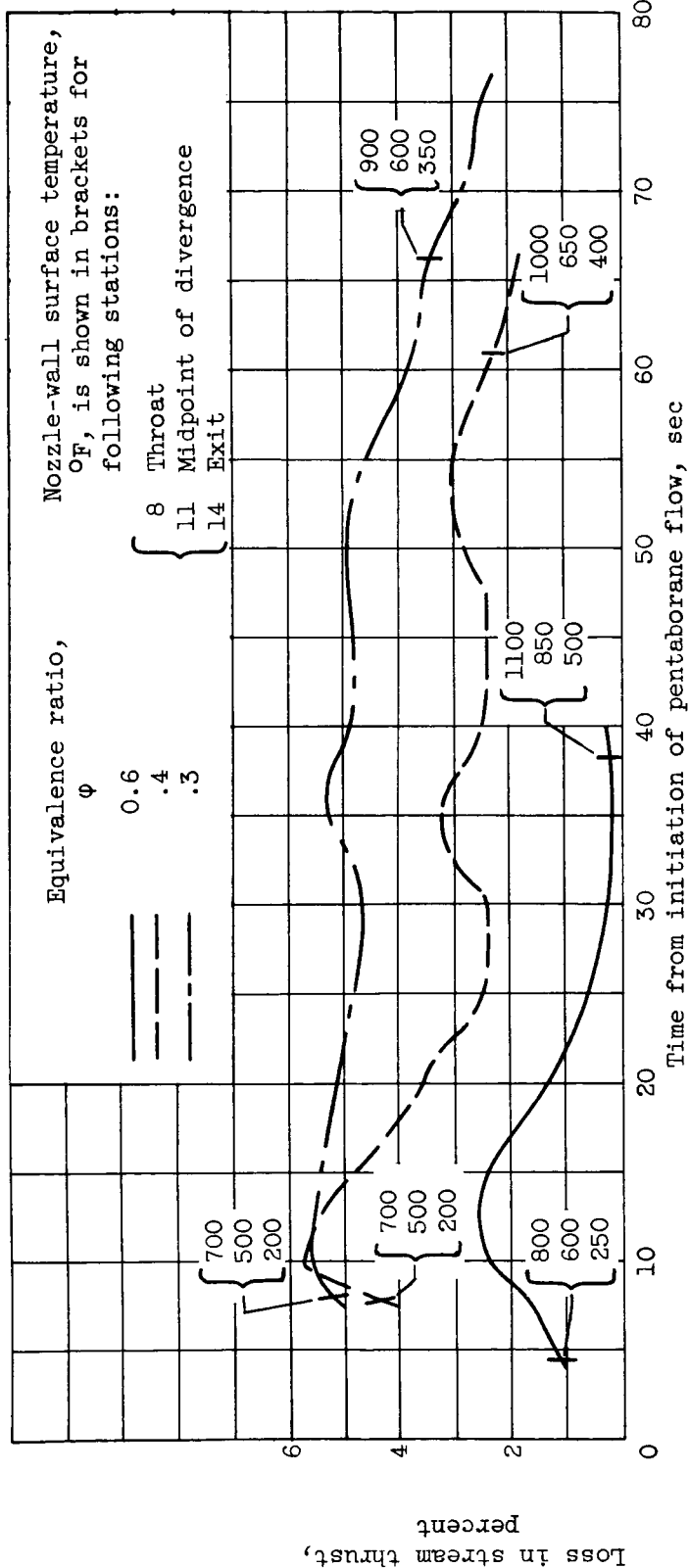


Figure 25. - Correlation of nozzle-wall temperature with loss in nozzle-exit stream thrust resulting from frictional resistance of boric-oxide films on divergent surface of nozzle.

CONFIDENTIAL